Supplementary Information

Photoactive Four-Coordinate Copper(I) Complexes Based on Chelating Diimine, Diphosphine, and Diisocyanide Ligands with High Excited-State Energies

*Tim H. Eggenweiler,[a] Alessandro Prescimone,[b] Daniel Häussinger,[a] and Oliver S. Wenger[a, *]*

[a] Department of Chemistry, University of Basel, St. Johanns-Ring 19, 4056 Basel, Switzerland

[b] Department of Chemistry, University of Basel, BPR 1096, Mattenstrasse 24a, 4058 Basel, Switzerland

Table of contents

1 Materials and methods:

All commercially available chemicals were used as received without further purification. Solvents for spectroscopic measurements were purchased as "extra dry" (99.8% purity) and filtered prior to use. The phosphine ligand, xantphos, was obtained commercially and used as received. The phenanthroline ligand was synthesized from 1,10-phenanthroline following a literature procedure.[1, 2] The isocyanide ligand was synthesized from 1,3-dibromobenzene and 2,6-dibromo-4-*tert*-butylaniline and following a literature procedure.[3]

Thin layer chromatography (TLC) was performed on pre-coated aluminum plates (silica gel 60 F254, 0.25 mm thickness). Visualization of compounds was achieved under UV light (254 nm). Column chromatography was performed on silica gel (silica gel 60, 40-63 µm, 230-400 mesh) using a Biotage One flash chromatography system with normal-phase silica cartridges.

NMR spectra were recorded on a Bruker Avance III NMR spectrometer operating at proton frequencies of 250 MHz, 400 MHz or 500 MHz. If not stated otherwise, 5mm diameter tubes at 298 K were used. Chemical shift values are reported in δ values relative to tetramethylsilane and were referenced to residual solvent signals as reported previously.[4] Coupling patterns were denoted as follows: s = singlet, d = doublet, t = triplet, m = multiplet, dd = doublet of doublets.

The temperature dependent NMR study was performed on a Bruker Avance III NMR spectrometer operating at 600.13 MHz proton frequency. The instrument was equipped with an indirect 5-mm BBI probe with self-shielded z-gradient. Chemical shifts are given in δ scale relative to tetramethylsilane as 0.00 ppm and were referenced to residual protonated solvent peaks (tetra-chloroethylene-d_2: ^{1}H: 6.00 ppm, ^{13}C: 73.578 ppm). The experiments were performed at 298 K or at the temperature stated. Temperatures were calibrated using methanol/glycerol standards showing accuracy within +/- 0.2 K. A high concentration (40-50 mM) was needed to resolve the ^{13}C NMR spectrum in good quality.

Elemental analysis was performed by Sylvie Mittelheisser, with a Vario Micro Cube instrument from Elementar. Residual solvent observed in the elemental analysis of all four complexes likely originates from solvent molecules incorporated into the crystal structures and therefore cannot be removed under vacuum. HRMS analyses were conducted by Dr. Michael Pfeffer on a Bruker maxis 4G ESI-Q-TOF under direct injection conditions with acetonitrile as solvent.

A suitable crystal was selected and mounted on a MITIGEN holder in perfluoroether oil on a STOE STADIVARI or STOE STADIVARI Cu diffractometer. The crystal was kept at a steady T = 150 K during data collection. The structure was solved with the ShelXT 2018/2[5] solution program using dual methods and by using Olex2 1.5[6] as the graphical interface. The model was refined with ShelXL 2018/3[7] using full matrix least squares minimisation on $\boldsymbol{F^2}$.

Cyclic voltammetry was performed in a glass cell containing 10 mM substrate and 100 mM tetra-*n*-butylammonium hexafluorophosphate as the supporting electrolyte in deaerated dry acetonitrile under an argon atmosphere. A platinum electrode was used for **[CuL^{CC}L^{NN}]$^+$** and a gold electrode for **[CuL^{NN}L^{PP}]$^+$**, **[CuL^{CC}L^{PP}]$^+$** and **[CuL^{CC}L^{CC}]$^+$** was used as the working electrode, a silver wire as the counter electrode and a saturated calomel electrode (SCE) as the reference electrode. A Versastat3-200 potentiostat (Princeton Applied Research) was used with a potential scan rate of 50 mV/s. Disk-shaped working electrodes had a diameter of approximately 1 mm. The oxidation potential was determined from the peak current as all complexes display irreversible oxidation events.

All spectroscopic measurements were performed at 298 K in 1 cm screw cap quartz cuvettes with septum caps. All solutions were deaerated using argon. Optical absorption spectra were recorded using a Cary 5000 spectrophotometer from Agilent Technologies. Steady-state luminescence spectra were recorded on a Fluorolog-322 from Horiba Jobin-Yvon, equipped with a Xenon lamp 450-Watt illuminator (FL-1039A/40A) and a water-cooled photomultiplier tube (PMT Hamamatsu R2658 or R928). The luminescence spectra were corrected for the spectral response of the system.

Time-resolved luminescence, photoluminescence lifetime studies and UV-vis transient absorption spectra were recorded on a LP920-KS apparatus from Edinburgh Instruments. A frequency-tripled pulsed Nd:YAG laser (Quantel Qsmart 450, ca. 10 ns pulse width) with a beam expander (BE02-355 from Thorlabs) in the beam path was used for excitation at 355 nm (pulse energy of ~ 30 mJ). Detection of transient UV-Vis absorption spectra occurred on an iCCD camera from Andor and single-wavelength kinetics were recorded with a photomultiplier tube.

Photoluminescence lifetime studies were performed on a LifeSpec II spectrometer (time-correlated single photon counting (TCSPC) technique) from Edinburgh Instruments with a temperature-controlled cuvette holder (TC 1, Quantum Northwest). For excitation either a

picosecond pulsed laser diode (375 nm) or a pulsed LED (310 nm) from Edinburgh Instruments was used.

Steady-state emission spectra of the powder samples were recorded on a Compact Fluorescence Lifetime Spectrometer from Hamamatsu (C11367). Solid-state quantum yields were recorded on an Absolute PL Quantum Yield Spectrometer from Hamamatsu (C11347).

2 Synthetic procedures

2.1 Synthesis of the copper(I)-complexes

$[CuL^{NN}L^{PP}]BF_4$

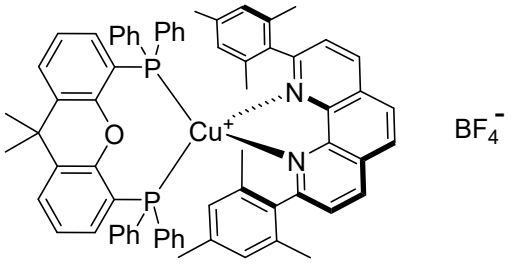

Under N_2, $[Cu(CH_3CN)_4]BF_4$ (50.0 mg; 159 μmol; 1.00 eq.) was dissolved in dry DCM (30 mL). Xantphos (96.6 mg; 167 μmol; 1.05 eq.) was added and the mixture was stirred for 1 h. Later 2,9-dimesityl-1,10-phenanthroline (69.5 mg; 167 μmol; 1.05 eq.) was added and stirred for an additional 1 h. The solution was concentrated to approximately one-fifth of its original volume under reduced pressure. Addition of *n*-hexane induced the formation of a yellow precipitate. The solution was collected by decantation and washed with a small amount of *n*-hexane. The product was obtained as a yellow, crystalline solid (123 mg; 107 μmol; 68 %).

^{1}H NMR (500 MHz, CD_2Cl_2) δ 8.49 (d, *J* = 8.2 Hz, 1H), 8.28 (d, *J* = 8.3 Hz, 1H), 7.86 (d, *J* = 8.8 Hz, 1H), 7.72 (d, *J* = 8.7 Hz, 1H), 7.59 (d, *J* = 8.2 Hz, 1H), 7.59 (d, *J* = 7.8 Hz, 2H), 7.47 (d, *J* = 8.2 Hz, 1H), 7.31 (t, *J* = 7.5 Hz, 2H), 7.17 (t, *J* = 7.5 Hz, 2H), 7.10 – 7.01 (m, 6H), 6.91 - 6.87 (m, 4H), 6.75 (s, 2H), 6.47 – 6.40 (m, 4H), 6.39 – 6.35 (m, 4H), 6.34 – 6.31 (m, 2H), 6.28 (s, 2H), 2.31 (s, 3H), 2.06 (s, 3H), 2.02 (s, 3H), 1.92 (s, 6H), 1.51 (s, 6H), 1.21 (s, 3H).

^{13}C{^{1}H} NMR (126 MHz, CD_2Cl_2) δ 162.4, 160.9, 153.6 (t, *J* = 6.3 Hz), 145.7, 144.7, 139.8, 138.8, 137.8, 137.5, 137.1, 136.9, 134.8, 133.5 (t, *J* = 7.7 Hz), 132.9 (t, *J* = 7.3 Hz), 132.8 (t, *J* = 1.8 Hz), 131.7 (t, *J* = 13.2 Hz), 130.8, 130.6 (t, *J* = 15.6 Hz), 130.4, 130.0, 129.9, 128.9, 128.8, 128.7 (t, *J*

= 4.7 Hz), 128.4 (t, *J* = 4.2 Hz), 128.3, 128.3, 127.7, 127.7, 127.6, 127.5, 124.9 (t, *J* = 2.3 Hz), 121.3 (t, *J* = 11.5 Hz), 35.7 (t, *J* = 1.6 Hz), 34.3, 24.6, 22.1, 21.6, 21.4, 20.4.

$^{31}P\{^{1}H\}$ NMR (202 MHz, CD_2Cl_2) δ -14.90.

$^{19}F\{^{1}H\}$ NMR (471 MHz, CD_2Cl_2) δ -153.21 (^{10}BF), -153.26 (^{11}BF).

^{11}B NMR (128 MHz, CD_2Cl_2) δ -1.05.

ESI-HRMS (m/z): calc. for $[CuL^{NN}L^{PP}]^+$: 1057.3464; found: 1057.3471.

EA: calc. for $C_{69}H_{60}N_2OBCuF_4P_2 \cdot 2.0\ CH_2Cl_2$: C, 64.83; H, 4.90; N, 2.13; found: C, 65.09; H, 4.73; N, 2.16.

$[CuL^{CC}L^{PP}]BF_4$

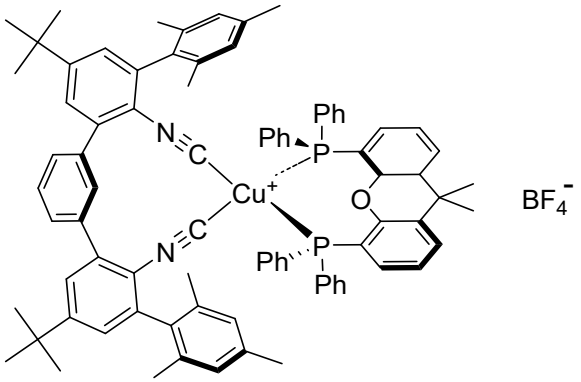

Under N_2, $[Cu(CH_3CN)_4]BF_4$ (47.6 mg; 151 μmol; 1.00 eq.) was dissolved in dry DCM (30 mL). Xantphos (92.0 mg; 159 μmol; 1.05 eq.) was added and the mixture was stirred for 1 h. Later 5',5'''-di-*tert*-butyl-2',2'''-diisocyano-2,2'''',4,4'''',6,6''''-hexamethyl-1,1':3',1'':3'',1''':3''',1''''-quinquephenyl (100 mg; 159 μmol; 1.05 eq.) was added and stirred for an additional 1 h. The solution was concentrated to approximately one-fifth of its original volume under reduced pressure. Addition of *n*-hexane induced the formation of a yellow precipitate. The solution was collected by decantation and washed with a small amount of *n*-hexane. The product was obtained as a yellow, crystalline solid (106 mg; 77.9 μmol; 52 %).

^{1}H NMR (600 MHz, 278 K, $C_2D_2Cl_4$) δ 8.00 (H_{20}), 7.83 ($H_{19'}$), 7.82 (H_{21}), 7.69 (H_{19}), 7.62 (H_{33}), 7.58 ($H_{33'}$), 7.55 (H_{25}), 7.45 ($H_{13'}$), 7.39 ($H_{25'}$), 7.37 (H_{13}), 7.36 (H_{24}), 7.22 (H_{11}), 7.21 ($H_{11'}$), 7.19 (H_{29}), 7.14 ($H_{24'}$), 7.10 (H_{34}), 7.07 (H_1), 7.05 ($H_{29'}$), 7.02 ($H_{34'}$), 6.91(H_{28}), 6.85 ($H_{28'}$), 6.79 ($H_{23'}$), 6.77 (H_{23}), 6.72 ($H_{1'}$), 6.67 ($H_{27'}$), 6.35 (H_{27}), 6.30 (H_3), 6.17 ($H_{35'}$), 6.15 (H_{35}),

5.95 ($H_{3'}$), 2.12 (H_7), 2.06 (H_8), 2.03 ($H_{9'}$), 2.00 (H_{37}), 1.98 ($H_{8'}$), 1.40 (H_9), 1.37 ($H_{37'}$), 1.32 ($H_{17'}$), 1.31 ($H_{17'}$), 1.20 ($H_{7'}$).

$^{13}C\{^1H\}$ NMR (151 MHz, 278 K, $C_2D_2Cl_4$) δ 154.5 (C_{12}), 154.4 ($C_{12'}$), 153.6 (C_{31}), 153.5 ($C_{31'}$), 139.5 ($C_{14'}$), 139.0 (C_{10}, $C_{10'}$, C_{14}), 138.0 (C_{18}), 137.6 (C_2), 137.5 ($C_{18'}$), 137.3 ($C_{2'}$), 135.7 (C_4), 135.3 ($C_{4'}$, C_6) 135.0 ($C_{6'}$), 133.9 ($C_{23'}$), 133.4 (C_5), 132.9 (C_{32}), 132.73 (C_{23}), 132.66 ($C_{5'}$), 132.44 ($C_{32'}$), 132.42 (C_{22}), 131.6 (C_{27}), 131.1 ($C_{22'}$), 131.0 ($C_{27'}$), 130.9 (C_{33}, C_{35}), 130.6 (C_{20}), 130.34 ($C_{26'}$), 130.28 ($C_{25'}$), 130.2 (C_{25}), 130.1 ($C_{35'}$), 130.0 (C_{19}), 129.8 ($C_{19'}$), 129.7 (C_{21}), 129.3 (C_{29}), 129.12 ($C_{24'}$), 129.05 ($C_{29'}$), 128.7 (C_{24}), 128.60 (C_{26}), 128.55 (C_3), 128.4 (C_{28}), 128.1 ($C_{28'}$), 127.99 ($C_{1'}$), 127.97 ($C_{11'}$),127.95 (C_1), 127.5 (C_{13}), 127.44 (C_{11}), 127.41 ($C_{13'}$), 127.2 ($C_{3'}$), 126.6 ($C_{33'}$), 124.7 (C_{34}), 124.5 ($C_{34'}$), 120.1 ($C_{30'}$), 119.4 (C_{15}), 119.2 (C_{30}), 119.1 ($C_{15'}$), 35.5 (C_{36}), 35.11 ($C_{16'}$), 35.09 (C_{16}), 33.0 ($C_{37'}$), 30.9 (C_{17}, $C_{17'}$), 23.6 (C_{37}), 21.7 ($C_{8'}$), 21.2 (C_8), 20.8 ($C_{7'}$), 20.4 (C_7), 19.7 (C_9), 18.6 ($C_{9'}$).

$^{31}P\{^1H\}$ NMR (243 MHz, 278 K, $C_2D_2Cl_4$) δ -5.7, -10.4.

$^{19}F\{^1H\}$ NMR (471 MHz, CD_2Cl_2) δ -153.38 (^{10}BF), -153.44 (^{11}BF).

^{11}B NMR (128 MHz, CD_2Cl_2) δ -1.08.

ESI-HRMS (m/z): calc. for $[CuL^{CC}L^{PP}]^+$: 1269.5042; found: 1269.5053.

EA: calc. for $C_{85}H_{80}N_2OBCuF_4P_2 \cdot 1.0\ CH_2Cl_2$: C, 71.59; H, 5.73; N, 1.94; found: C, 71.42; H, 5.63; N, 1.84.

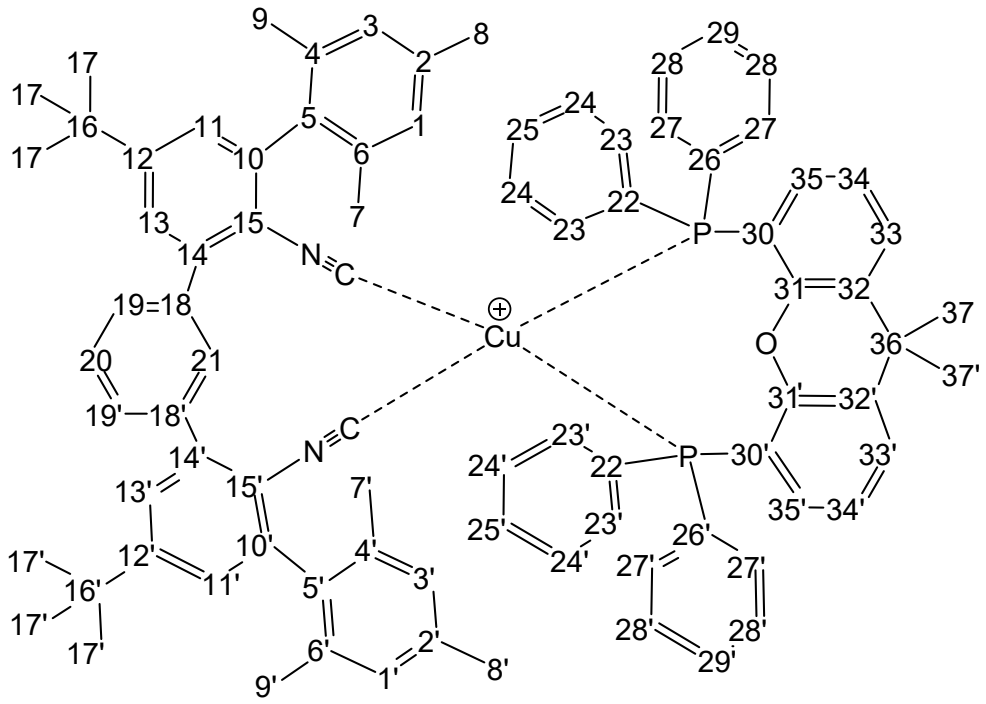

Figure S1: Atom numbering scheme of ***[CuL^{CC}L^{PP}]$^{+}$****. Atoms that are chemically equivalent but become non-equivalent on the NMR timescale are distinguished by a prime (').*

[CuL^{CC}L^{NN}]BF$_4$

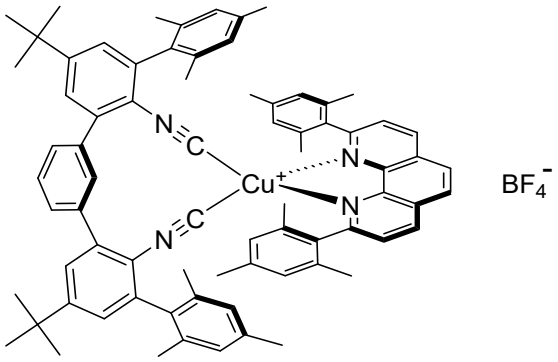

Under N_2, $[Cu(CH_3CN)_4]BF_4$ (47.6 mg; 151 μmol; 1.00 eq.) was dissolved in dry DCM (30 mL). 2,9-Dimesityl-1,10-phenanthroline (66.2 mg; 159 μmol; 1.05 eq.) was added and the mixture was stirred for 1 h. Later 5',5'''-di-*tert*-butyl-2',2'''-diisocyano-2,2'''',4,4'''',6,6''''-hexamethyl-1,1':3',1'':3'',1''':3''',1''''-quinquephenyl (100 mg; 159 μmol; 1.05 eq.) was added and stirred for an additional 1 h. The solution was concentrated to approximately one-fifth of its original volume under reduced pressure. Addition of *n*-hexane induced the formation of a yellow precipitate. The solution was collected by decantation and washed with a small amount of *n*-hexane. The product was obtained as a yellow, crystalline solid (119 mg; 99.8 μmol; 66 %).

^{1}H NMR (500 MHz, CD_2Cl_2) δ δ 8.57 (d, *J* = 8.3 Hz, 2H), 8.13 (s, 2H), 7.87 (t, *J* = 7.8 Hz, 1H), 7.55 (d, *J* = 8.2 Hz, 2H), 7.46 (d, *J* = 7.5 Hz, 2H), 7.42 (s, 1H), 7.36 (s, 2H), 7.20 (s, 2H), 6.98 (s, 2H),

6.71 (s, 2H), 6.58 (s, 4H), 2.27 (s, 6H), 2.16 (s, 6H), 2.08 (s, 6H), 1.70 (s, 12H), 1.34 (s, 18H), 1.26 (s, 6H).

$^{13}C\{^{1}H\}$ NMR (126 MHz, CD_2Cl_2) δ 161.5, 154.2, 148.6, 143.7, 140.4, 138.3, 138.3, 138.1, 136.1, 134.2, 130.9, 130.5, 128.9, 128.6, 128.4, 128.2, 127.9, 127.0, 120.3, 35.4, 31.1, 21.6, 21.0, 19.8, 19.3.

$^{19}F\{^{1}H\}$ NMR (376 MHz, CD_2Cl_2) δ -153.12 (^{10}BF), -153.17 (^{11}BF).

^{11}B NMR (128 MHz, CD_2Cl_2) δ -1.03.

ESI-HRMS (m/z): calc. for $[CuL^{CC}L^{NN}]^+$: 1107.5366; found: 1107.5378.

EA: calc. for $C_{76}H_{76}N_4BCuF_4 \cdot 1.0\ CH_2Cl_2$: C, 72.21; H, 6.14; N, 4.37; found: C, 72.13; H, 6.18; N, 4.28.

$[CuL^{CC}L^{CC}]BF_4$

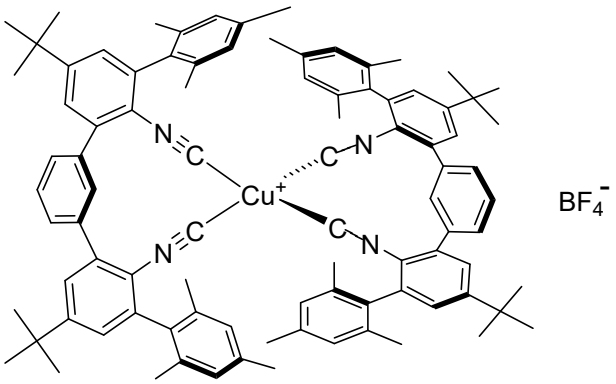

Under N_2, $[Cu(CH_3CN)_4]BF_4$ (47.6 mg; 151 μmol; 1.00 eq.) was dissolved in dry DCM (30 mL). 5',5'''-Di-*tert*-butyl-2',2'''-diisocyano-2,2'''',4,4'''',6,6''''-hexamethyl-1,1':3',1'':3'',1''':3''',1''''-quinquephenyl (200 mg; 318 μmol; 1.10 eq.) was added and the mixture was stirred for 1 h. The solution was concentrated to approximately one-fifth of its original volume under reduced pressure. Addition of *n*-hexane induced the formation of a yellow precipitate. The solution was collected by decantation and washed with a small amount of *n*-hexane. The product was obtained as a white, crystalline solid (192 mg; 146 μmol; 96 %).

^{1}H NMR (500 MHz, CD_2Cl_2) δ 7.70 (t, *J* = 7.7 Hz, 2H), 7.49 (dd, *J* = 7.7, 1.5 Hz, 4H), 7.44 (t, *J* = 1.6 Hz, 2H), 7.42 (s, 2H), 7.38 (s, 2H), 7.33 (s, 2H), 7.25 (s, 2H), 7.01 (s, 4H), 6.89 (s, 2H), 6.78 (s, 2H), 2.36 (s, 6H), 2.16 (s, 6H), 2.00 (s, 12H), 1.89 (s, 12H), 1.38 (s, 18H), 1.33 (s, 18H).

$^{13}C\{^{1}H\}$ NMR (126 MHz, CD_2Cl_2) δ 154.5, 139.9, 138.8, 137.9, 137.6, 135.7, 133.5, 129.8, 129.6, 128.8, 128.4, 128.0, 127.4, 127.1, 120.1, 35.2, 30.8, 20.8, 19.7.

$^{19}F\{^{1}H\}$ NMR (471 MHz, CD_2Cl_2) δ -153.52 (^{10}BF), -153.58 (^{11}BF).

^{11}B NMR (128 MHz, CD_2Cl_2) δ -1.15.

ESI-HRMS (m/z): calc. for $[CuL^{CC}L^{CC}]^+$: 1319.6931; found: 1319.6944.

EA: calc. for $C_{92}H_{96}N_4BCuF_4 \cdot 0.4\ CH_2Cl_2$: C, 76.96; H, 6.77; N, 3.89; found: C, 76.94; H, 6.75; N, 3.94.

2.2 Photocatalysis

[2+2] cycloaddition of norbornadiene to quadricyclane:

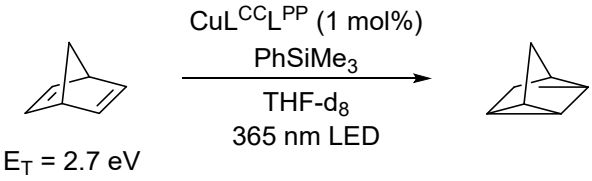

Norbornadiene (9.2 mg, 100 µmol) and trimethyl(phenyl)silane (5.0 mg, 33 µmol) were dissolved in THF-d_8 (1.2 mL). The solution was split in two parts and to one part was **[CuL^{CC}L^{PP}]$^+$** added. Then both parts were transferred to a separate Young NMR tube and degassed by three freeze-pump-thaw cycles. Afterwards both samples were irradiated parallel with a Thorlabs LED lamp (365 nm). The samples were measured after each period, one hour, and the yields were referenced to the internal standard.

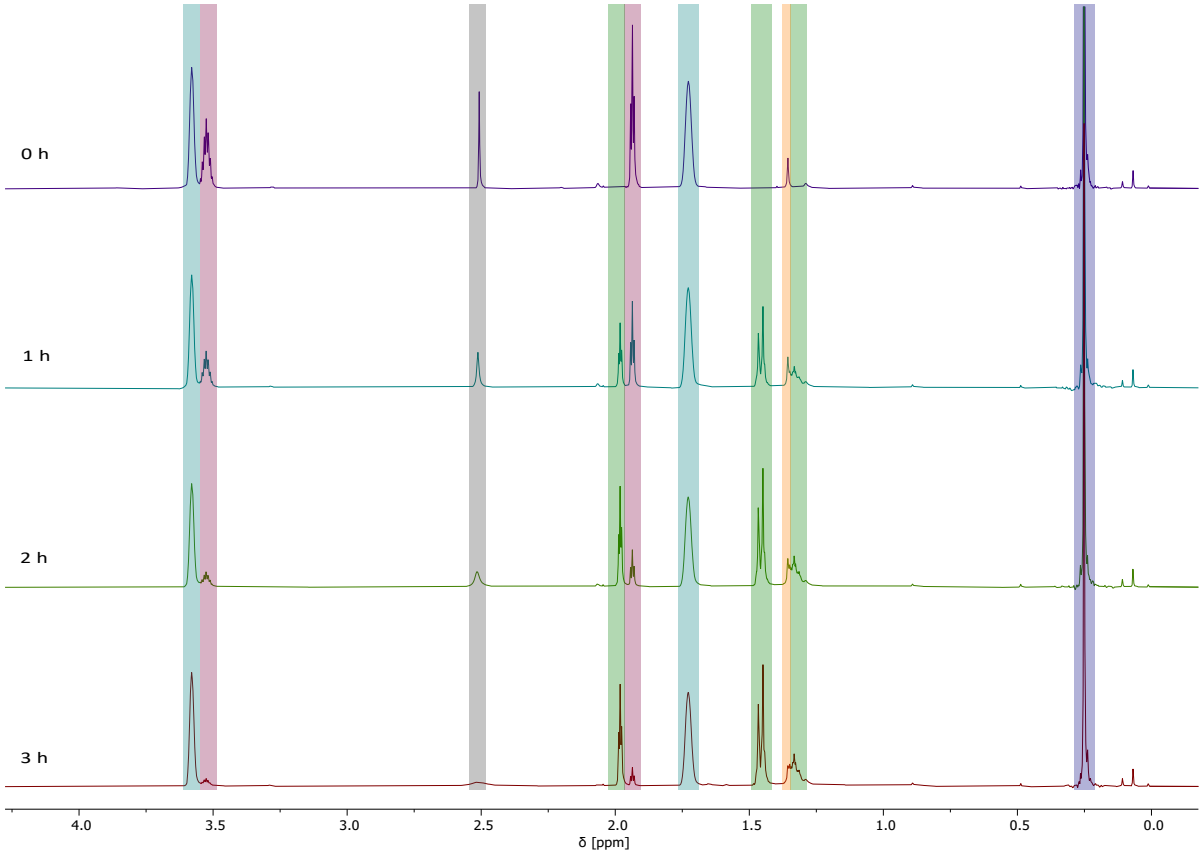

*Figure S2: ^{1}H-NMR spectrum of a solution of norbornadiene (50 µmol), **[CuL^{CC}L^{PP}]$^+$** (1 mol%) as the catalyst and trimethyl(phenyl)silane (17 µmol) as the internal standard in deaerated THF-d_8 after the indicated irradiation times. The light source was an ultraviolet LED lamp (365 nm) at room temperature. The signals marked in red are due to the starting material norbornadiene and the signals in green due to the product quadricyclane. Further the signal in orange is due to **[CuL^{CC}L^{PP}]$^+$**. The signals in violet belong to the internal standard, trimethyl(phenyl)silane, in gray to water and in turquoise to THF-d_8.*

Table S1: Substrate conversion and product yield of the reaction of norbornadiene with ***[CuL^{CC}L^{PP}]$^{+}$*** *determined by integration of the relevant ^{1}H-NMR resonances.*

time	substrate (1.87 ppm; [%])	product (1.95 ppm; [%])
0 h	100	0
1 h	53	39
2 h	26	59
3 h	14	61

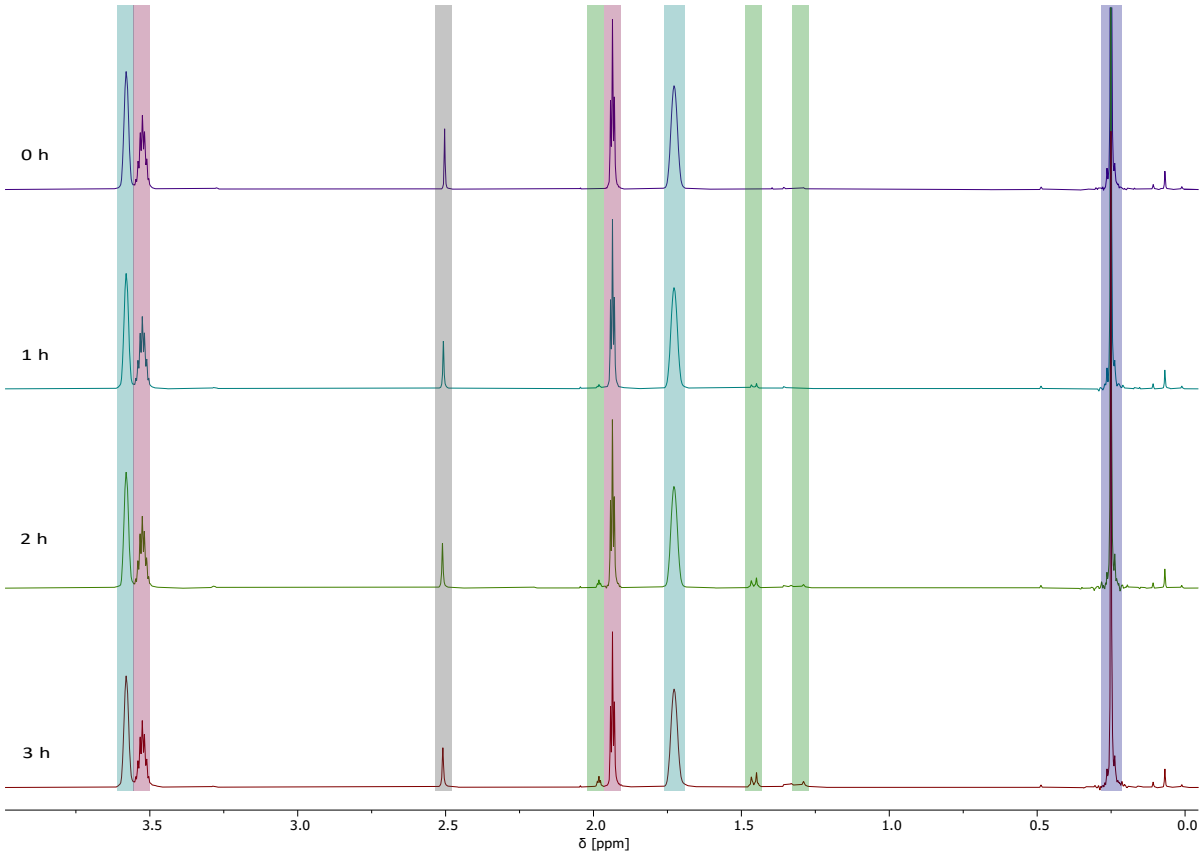

Figure S3: ^{1}H-NMR spectrum of a solution of norbornadiene (50 µmol) and trimethyl(phenyl)silane (17 µmol) as the internal standard in deaerated THF-d_8 after the indicated irradiation times. The light source was an ultraviolet LED lamp (365 nm) at room temperature. The signals marked in red are due to the starting material norbornadiene and the signals in green due to the product quadricyclane. The signals in violet belong to the internal standard, trimethyl(phenyl)silane, in gray to water and in turquoise to THF-d_8.

Table S2: Substrate conversion and product yield of the reaction of norbornadiene without ***[CuL^{CC}L^{PP}]$^{+}$*** *determined by integration of the relevant ^{1}H-NMR resonances.*

time	substrate (1.87 ppm; [%])	product (1.95 ppm; [%])
0 h	100	0
1 h	96	2
2 h	92	4
3 h	91	6

3 Luminescence lifetime measurements

The luminescence of **[CuL^{NN}L^{PP}]$^{+}$** displays a strong and well-defined emission band. In this case the emission exhibits a monoexponential decay in the luminescence lifetime measurement (Figure S4). For **[CuL^{CC}L^{CC}]$^{+}$** the emission also exhibits a monoexponential decay after correction of the measurement for the instrument response function (IRF). In contrast, biexponential decays were observed for **[CuL^{CC}L^{PP}]$^{+}$** and **[CuL^{CC}L^{NN}]$^{+}$**. **[CuL^{CC}L^{PP}]$^{+}$** and **[CuL^{CC}L^{NN}]$^{+}$** are showing only weak emissions and therefore required a broad detection bandwidth (20 nm for **[CuL^{CC}L^{PP}]$^{+}$** and 30 nm for **[CuL^{CC}L^{NN}]$^{+}$**).

For **[CuL^{CC}L^{PP}]$^{+}$** is an additional emission band at 350 nm of a photodegradation product (Figure S5) visible if not measured with a delay of 500 ns (Figure 3 of the main manuscript). The shift of the MLCT emission in Figure S5 compared to Figure 3 is due to the tail of the emission of the photodegradation product as well as due to two different measuring techniques, steady state emission spectra and time gated emission spectra. The emission of the photodegradation product also contributes to the luminescence decay; therefore, the decay traces were analysed with a delay of 500 ns (Figure S6). Under these conditions, a biexponential decay was observed, with the two lifetimes attributed to the conformers, which are also evident in the variable-temperature NMR studies (see SI, Section 8). In this work, the discussion focuses on the longer-lived component (4.45 µs), which is assigned to emission originating from the triplet state.

For **[CuL^{CC}L^{NN}]$^{+}$**, also an additional emission band from a photodegradation product (Figure S7) is observed, and a biexponential decay can be detected at 650 nm (Figure S8). The longer-lived component can be attributed to the emission of the MLCT state, which is not observed when the emission is detected at 450 nm (Figure S9).

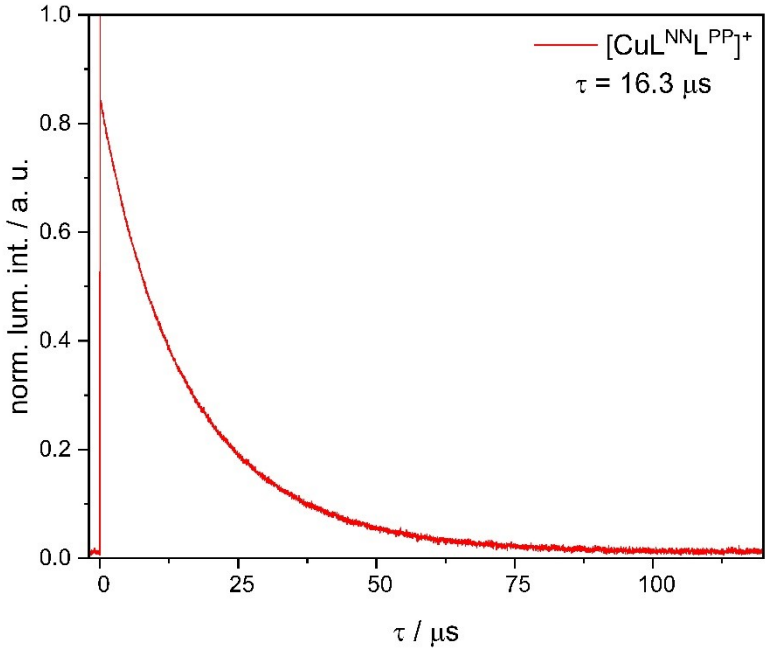

Figure S4: Emission intensity decay (λ_{exc} = 430 nm; λ_{em} = 540 nm) of ***[CuL^{NN}L^{PP}]$^{+}$*** *in dry, deaerated THF at 20 °C.*

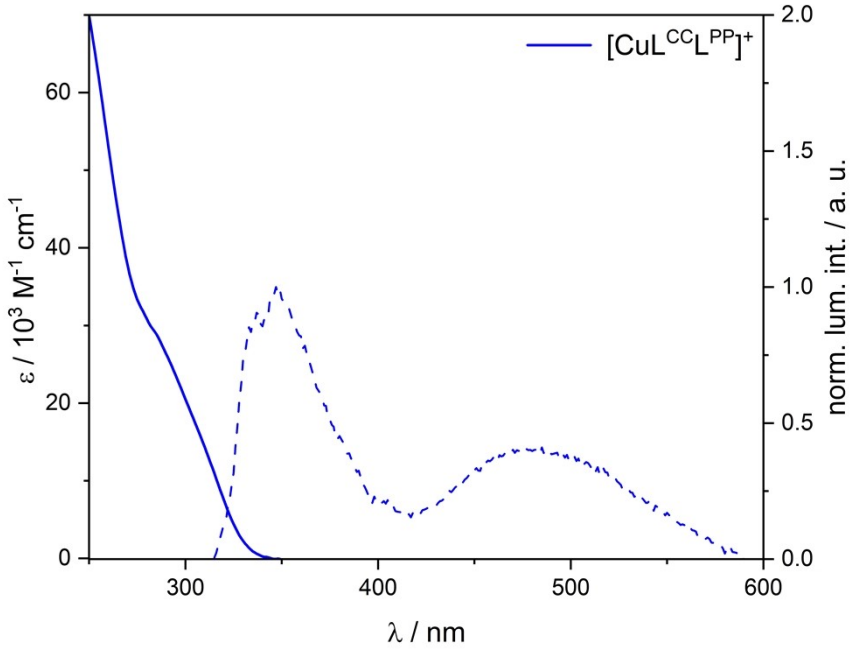

Figure S5: UV/Vis absorption spectra (solid lines) and emission spectra (dashed lines) of **[CuL^{CC}L^{PP}]$^{+}$** in dry, deaerated THF at 20 ° C. UV/Vis spectra were recorded at a concentration of 20 μM and converted to molar extinction coefficients (ε). The emission spectrum was recorded at 100 μM and normalized to the maximum intensity. **[CuL^{CC}L^{PP}]$^{+}$** was excited with continuous irradiation at 300 nm.

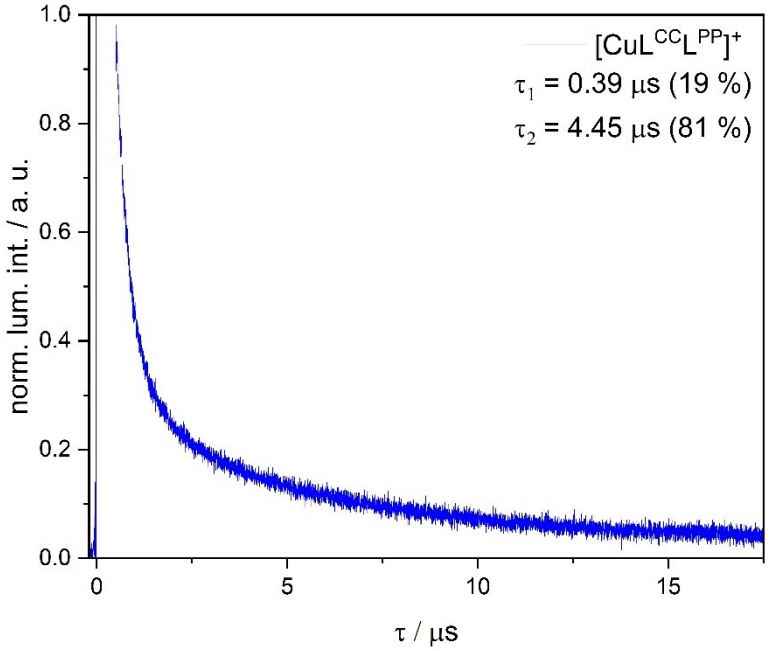

Figure S6: Emission intensity decay (λ_{exc} = 350 nm; λ_{em} = 550 nm) of ***[CuL^{CC}L^{PP}]$^+$*** *in dry, deaerated THF at 20 ° C. The spectrum is baseline corrected and normalized on the intensity after 500 ns.*

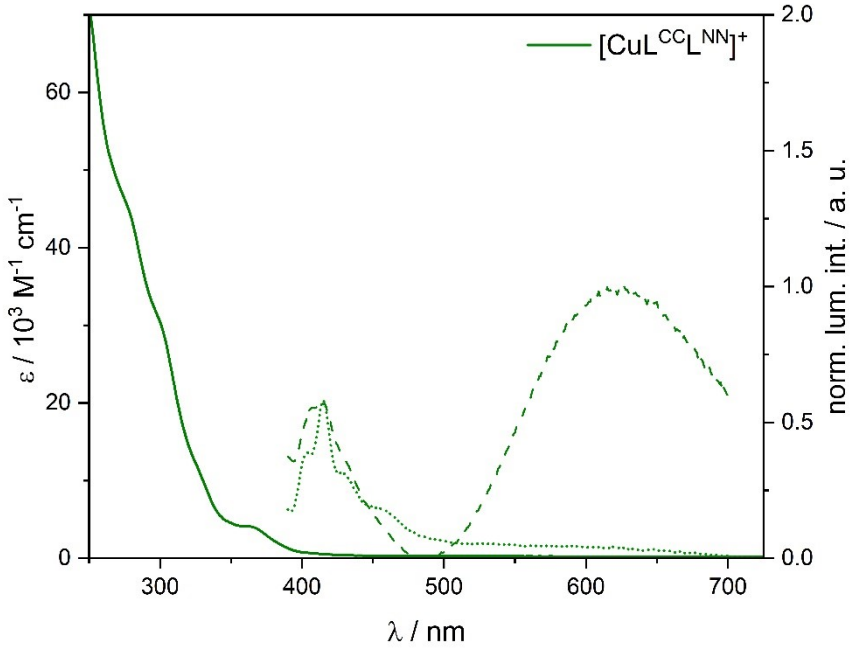

Figure S7: UV/Vis absorption spectra (solid lines) and emission spectra (dashed lines) of **[CuL^{CC}L^{NN}]$^+$** in dry, deaerated DCM at 20 ° C. The emission spectra (dotted) in dry, deaerated THF at 20° C is shown for comparison. UV/Vis spectra were recorded at a concentration of 20 μM and converted to molar extinction coefficients (ε). Emission spectra were recorded at 100 μM and normalized either to the maximum intensity in DCM or to the same intensity at 415 nm as the DCM spectrum for the THF measurement. Both emission spectra of **[CuL^{CC}L^{NN}]$^+$** were excited with continuous irradiation at 370 nm.

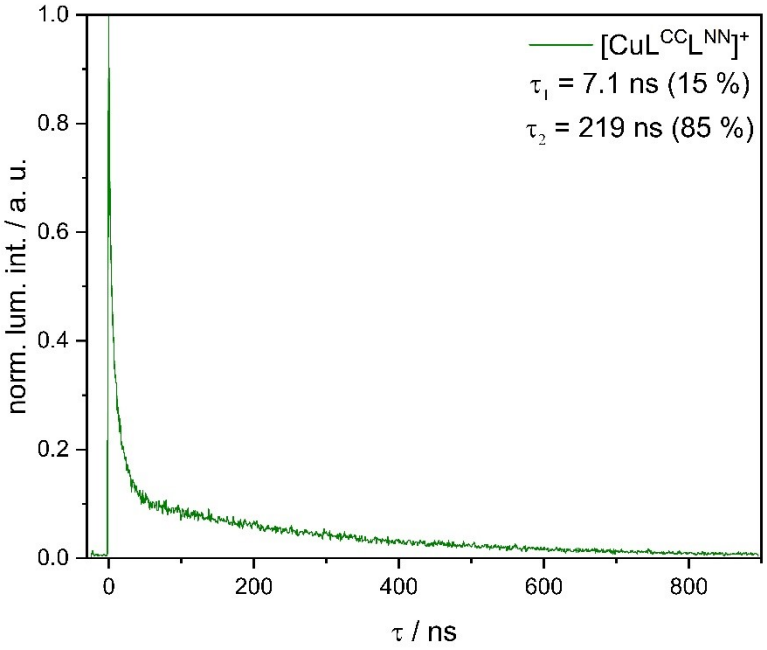

Figure S8: Emission intensity decay (λ_{exc} = 375 nm; λ_{em} = 650 nm) of ***[CuL^{CC}L^{NN}]$^{+}$*** *in dry, deaerated DCM at 20 °C.*

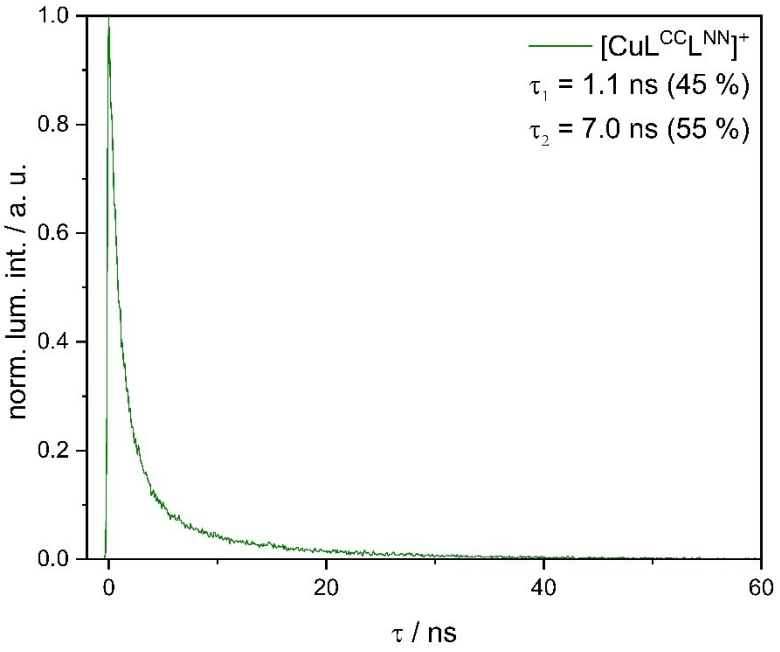

Figure S9: Emission intensity decay (λ_{exc} = 375 nm; λ_{em} = 450 nm) of ***[CuL^{CC}L^{NN}]$^{+}$*** *in dry, deaerated DCM at 20 °C.*

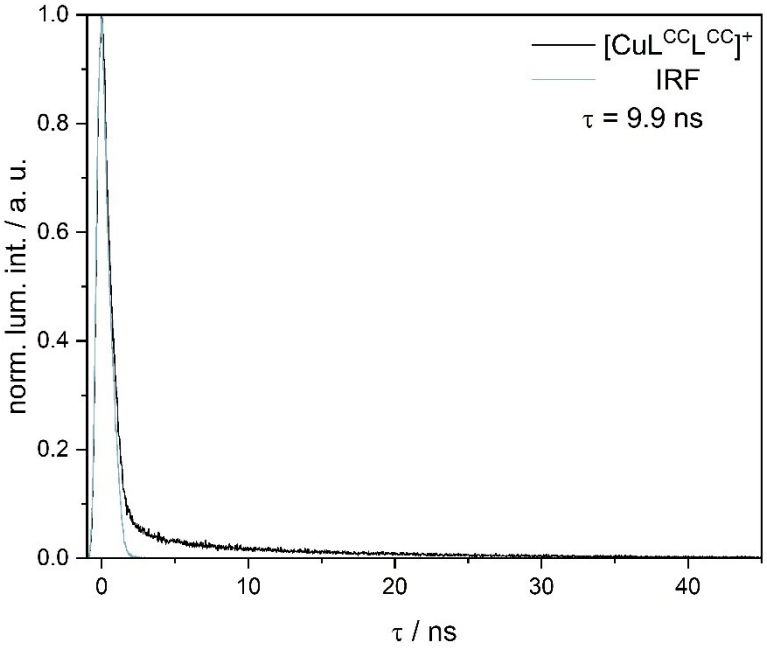

Figure S10: Emission intensity decay (λ_{exc} = 310 nm; λ_{em} = 350 nm) of ***[CuL^{CC}L^{CC}]$^{+}$*** *(black trace) in dry, deaerated THF at 20 °C. The instrument response function (IRF) is shown in light blue trace. The lifetime τ_1 (9.9 ns) is attributed to the decay of the ligand-centered (LC) state, while τ_2 (0.1 ns) is attributed to the IRF of the measurement.*

4 Luminescence in the solid state

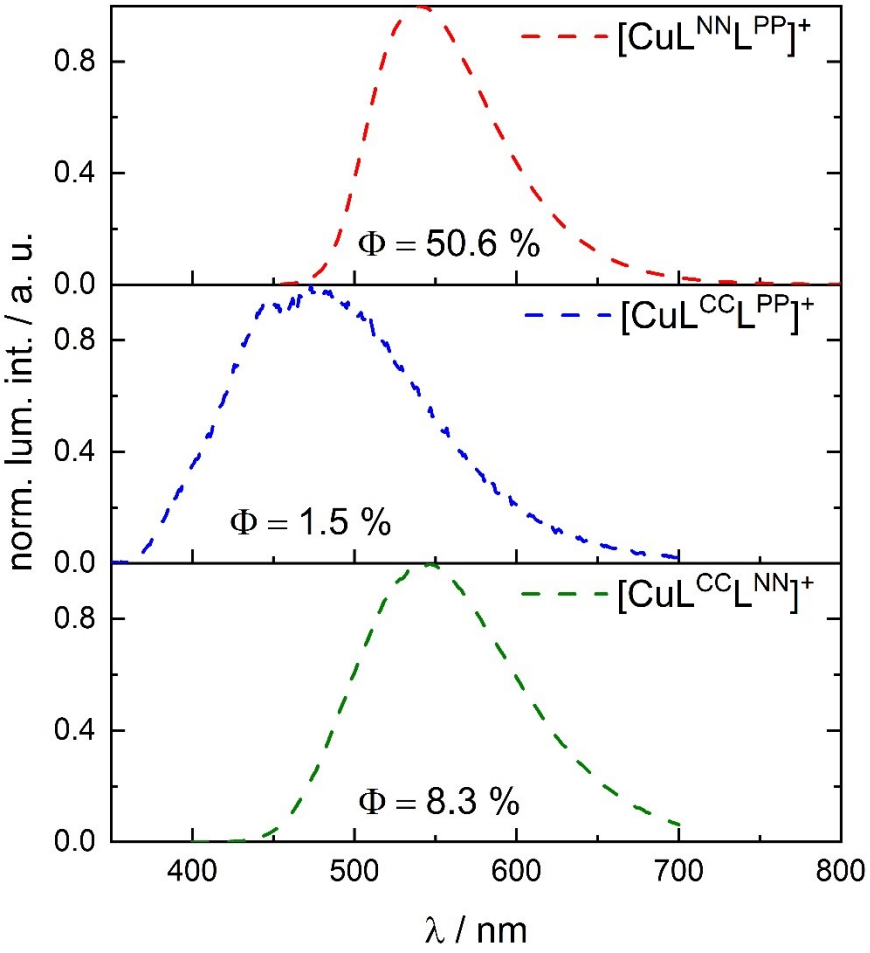

Figure S11: Solid-state emission spectra and the photoluminescence quantum yields (Φ) of ***[CuL^{NN}L^{PP}]$^{+}$***, ***[CuL^{CC}L^{PP}]$^{+}$*** *and* ***[CuL^{CC}L^{NN}]$^{+}$*** *were measured from the powder samples.* ***[CuL^{CC}L^{CC}]$^{+}$*** *shows no emission in the solid state. The complexes were excited using LEDs at the following wavelengths:* ***[CuL^{NN}L^{PP}]$^{+}$*** *at 405 nm,* ***[CuL^{CC}L^{PP}]$^{+}$*** *at 340 nm, and* ***[CuL^{CC}L^{NN}]$^{+}$*** *at 365 nm.*

5 Cyclic voltammetry

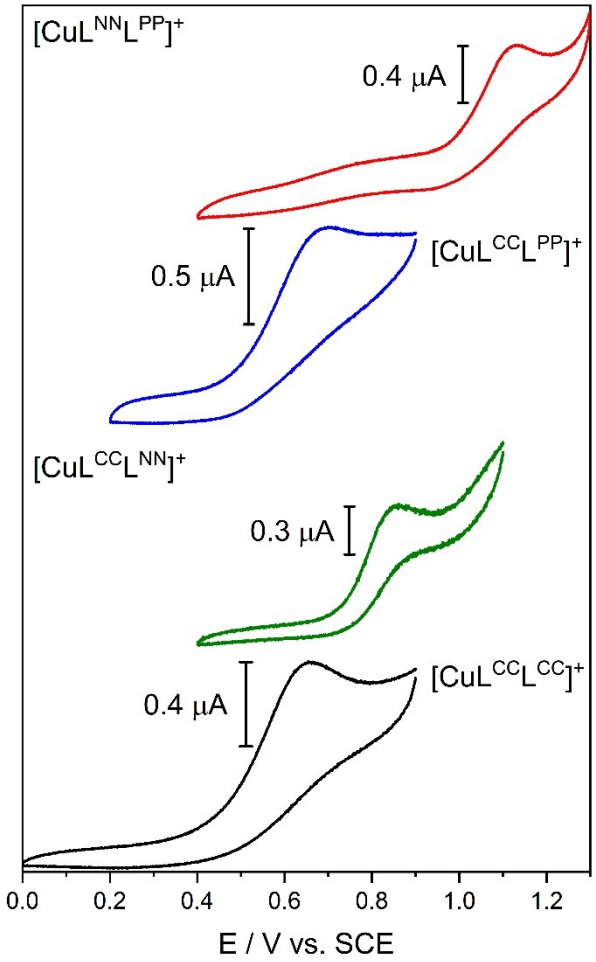

Figure S12: Cyclic voltammograms of 10 mM ***[CuL^{NN}L^{PP}]$^{+}$***, ***[CuL^{CC}L^{PP}]$^{+}$***, ***[CuL^{CC}L^{NN}]$^{+}$*** *and* ***[CuL^{CC}L^{CC}]$^{+}$*** *in dry, deaerated acetonitrile at 20 °C with 100 mM [NBu$_4$]PF$_6$ as supporting electrolyte. The scan rate was 0.05 V/s in all measurements.*

6 Triplet-triplet energy transfer

All triplet-triplet energy transfer measurements, including transient absorption and spectral emission, were performed by exciting the sample at 355 nm using a laser pulse energy of 30 mJ. All measurements were conducted with 100 µM **[CuL^{CC}L^{PP}]$^{+}$** in dry, deaerated THF. For the energy transfer experiment, 25 mM of 4,4'-dimethoxy-1,1'-biphenyl (**BP**) was added.

In the transient absorption spectrum of **[CuL^{CC}L^{PP}]$^{+}$** the dominant feature corresponds to the emission centered at 510 nm. A weak excited-state absorption is also observed at around 380 nm. This spectrum serves as a reference, as both features are quenched upon addition of **BP** to the solution, consistent with efficient triplet–triplet energy transfer.

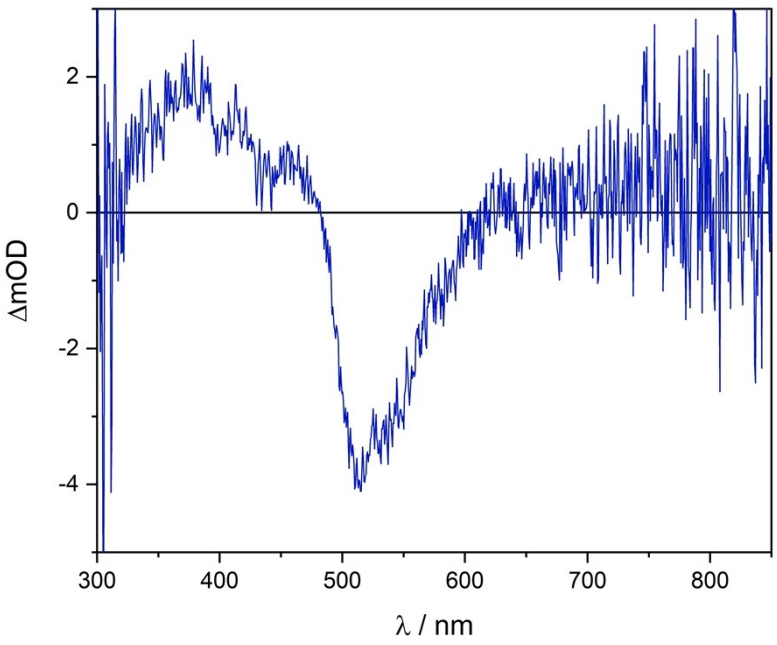

Figure S13: Transient absorption spectrum of 100 μM ***[CuL^{CC}L^{PP}]$^{+}$*** *in deaerated THF excited at 355 nm with 30 mJ laser pulse.*

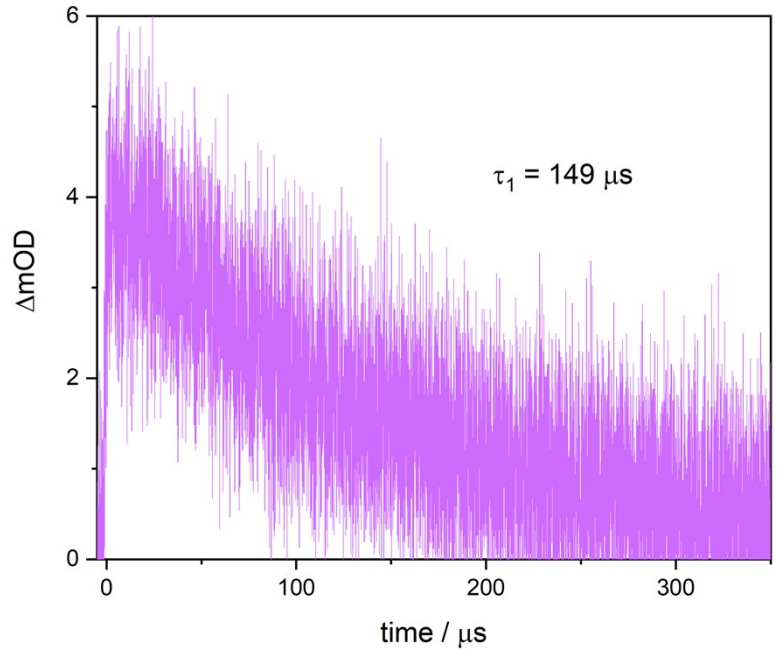

Figure S14: Transient absorption decay (λ_{exc} = 355 nm; λ_{abs} = 390 nm) of 100 μM ***[CuL^{CC}L^{PP}]$^{+}$*** *and 25 mM 4,4'-dimethoxy-1,1'-biphenyl in deaerated THF.*

7 X-ray crystallography

Suitable crystals of all four copper(I) complexes could be obtained as follows.

Single yellow block-shaped crystals of **[CuL^{NN}L^{PP}]$^{+}$** recrystallized from a mixture of THF and *n*-hexane by solvent layering. A suitable crystal with dimensions 0.22 × 0.21 × 0.21 mm^3 was selected.

Single colorless block-shaped crystals of **[CuL^{CC}L^{PP}]$^{+}$** recrystallized from a mixture of chloroform and *n*-hexane by solvent layering. A suitable crystal with dimensions 0.24 × 0.22 × 0.21 mm^3 was selected.

Single colorless plate-shaped crystals of **[CuL^{CC}L^{NN}]$^{+}$** recrystallized from a mixture of chloroform and *n*-hexane by solvent layering. A suitable crystal with dimensions 0.28 × 0.19 × 0.08 mm^3 was selected.

Single colorless block-shaped crystals of **[CuL^{CC}L^{CC}]$^{+}$** recrystallized from a mixture of 1,2-dimethoxyethane and diethyl ether by vapor diffusion. A suitable crystal with dimensions 0.2 × 0.19 × 0.17 mm^3 was selected.

Table S7: crystallographic parameters for ***[CuL^{NN}L^{PP}]$^+$, [CuL^{CC}L^{PP}]$^+$, [CuL^{CC}L^{NN}]$^+$*** *and* ***[CuL^{CC}L^{CC}]$^+$.***

Compound	**[CuL^{NN}L^{PP}]BF$_4$**	**[CuL^{CC}L^{PP}]BF$_4$**	**[CuL^{CC}L^{NN}]BF$_4$**	**[CuL^{CC}L^{CC}]BF$_4$**
Formula	$C_{75}H_{72}BCuF_4N_2O_{2.5}P_2$	$C_{91}H_{86}BCl_{18}CuF_4N_2OP_2$	$BC_{79.2}CuF_4H_{82.4}N_4O_{0.8}$	$C_{99.6}H_{115}BCuF_4N_4O_{3.8}$
CCDC number	2502158	2502159	2502160	2502161
$D_{calc.}$/ g cm^{-3}	1.294	1.386	1.241	1.115
μ/mm^{-1}	1.439	4.631	0.931	1.543
Formula Weight	1253.63	2074.00	1253.44	1579.30
Colour	yellow	colourless	colourless	colourless
Shape	block-shaped	block-shaped	plate-shaped	block-shaped
Size/mm^3	0.22×0.21×0.21	0.24×0.22×0.21	0.28×0.19×0.08	0.2×0.19×0.17
T/K	150	150	150	150
Crystal System	monoclinic	triclinic	monoclinic	monoclinic
Space Group	$P2_1/n$	P-1	$P2_1/c$	$P2_1/n$
a/Å	12.4724(3)	15.4453(3)	18.3390(3)	14.6955(4)
b/Å	24.5962(7)	17.0861(4)	14.3768(2)	26.9442(7)
c/Å	21.6817(5)	20.7269(5)	25.9417(5)	24.5086(6)
α/°	90	101.982(2)	90	90
β/°	104.631(2)	90.252(2)	101.1520(10)	104.195(2)
γ/°	90	111.204(2)	90	90
V/Å^3	6435.7(3)	4969.4(2)	6710.54(19)	9408.1(4)
Z	4	2	4	4
Z'	1	1	1	1
Wavelength/Å	1.54186	1.34143	1.54186	1.34143
Radiation type	Cu K$_\alpha$	Ga K$_\alpha$	Cu K$_\alpha$	Ga K$_\alpha$
Θ_{min}/°	3.736	2.680	3.531	5.57
Θ_{max}/°	70.122	55.818	73.111	108.998
Measured Refl's.	76163	83809	133785	121082
Indep't Refl's	12069	19132	13292	17611
Refl's I≥2 σ(I)	10208	12555	9079	13331
R_{int}	0.0263	0.1665	0.0756	0.1520
Parameters	816	1117	797	942
Restraints	75	115	137	135
Largest Peak	1.333	1.673	0.865	1.17
Deepest Hole	-1.165	-1.196	-0.977	-1.30
GooF	1.039	1.077	1.093	1.157
wR_2 (all data)	0.1836	0.2984	0.2582	0.2883
wR_2	0.1728	0.2745	0.2356	0.2730
R_1 (all data)	0.0737	0.1684	0.1470	0.1416
R_1	0.0625	0.1248	0.1136	0.1173

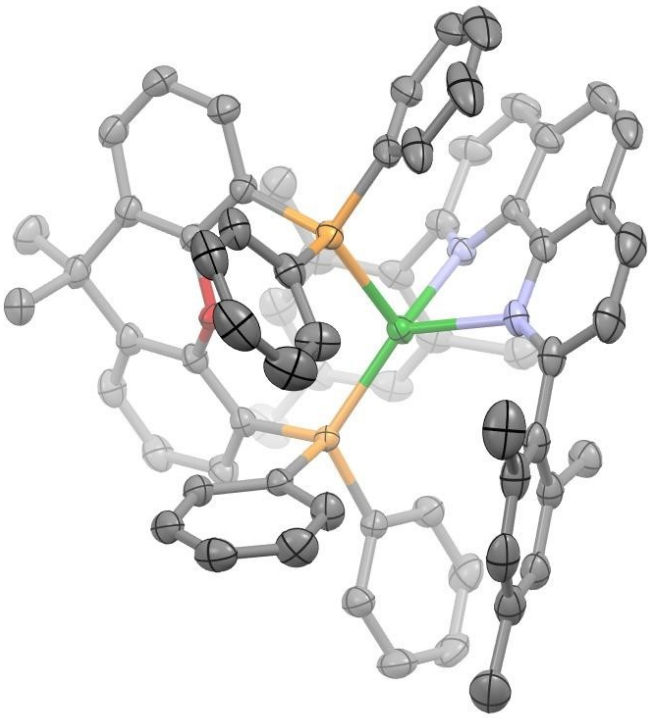

Figure S15: X-ray crystal structure of ***[CuL^{NN}L^{PP}]$^{+}$****. Ellipsoids are drawn at 50% probability. Hydrogen atoms and counterions are omitted for clarity. Depth cueing has been applied to enhance structural visualization. Ellipsoids are drawn at 50% probability. Hydrogen atoms and counterions are omitted for clarity. Depth cueing has been applied to enhance structural visualization.*

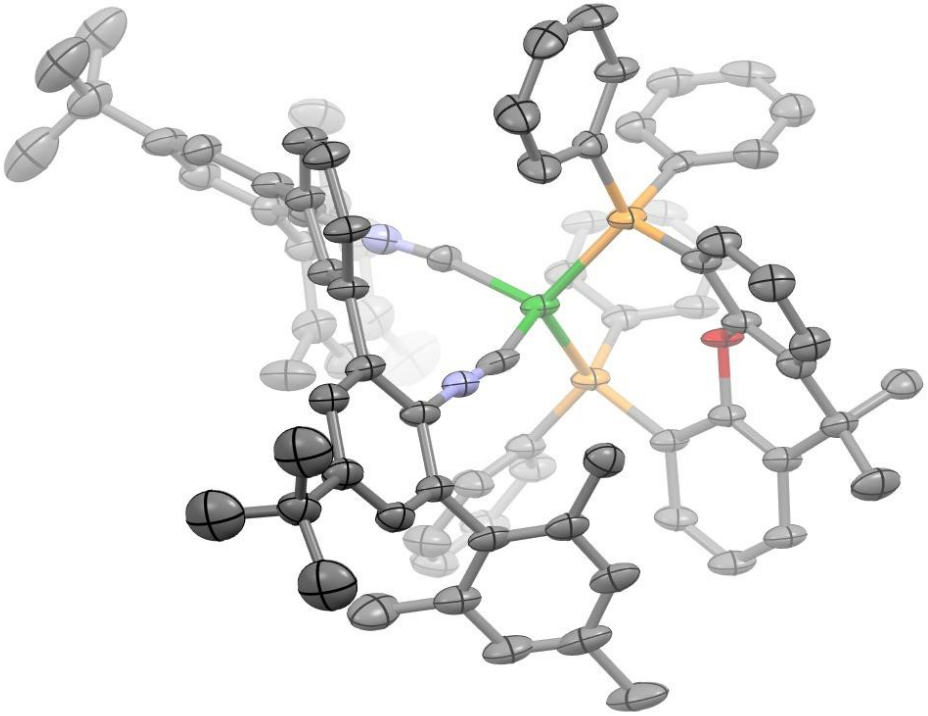

Figure S16: X-ray crystal structure of ***[CuL^{CC}L^{PP}]$^{+}$****. Ellipsoids are drawn at 50% probability. Hydrogen atoms and counterions are omitted for clarity. Depth cueing has been applied to enhance structural visualization. Ellipsoids are drawn at 50% probability. Hydrogen atoms and counterions are omitted for clarity. Depth cueing has been applied to enhance structural visualization.*

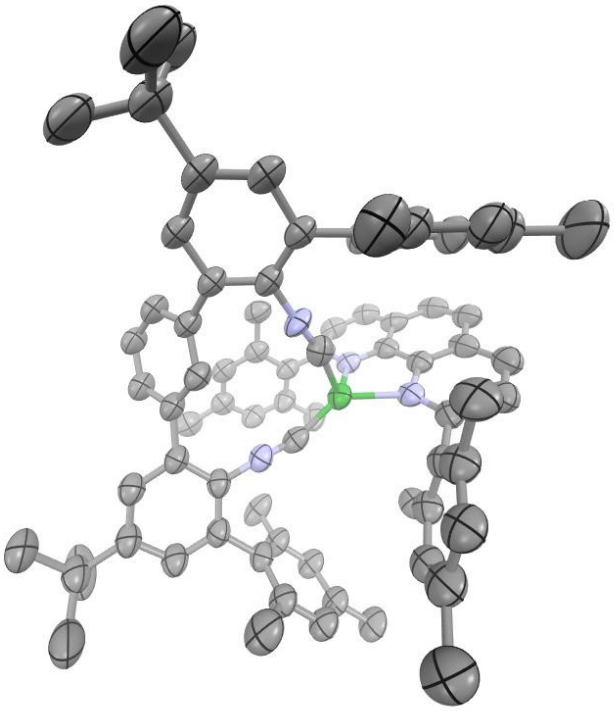

Figure S17: X-ray crystal structure of ***[CuL^{CC}L^{NN}]$^{+}$****. Ellipsoids are drawn at 50% probability. Hydrogen atoms and counterions are omitted for clarity. Depth cueing has been applied to enhance structural visualization. Ellipsoids are drawn at 50% probability. Hydrogen atoms and counterions are omitted for clarity. Depth cueing has been applied to enhance structural visualization.*

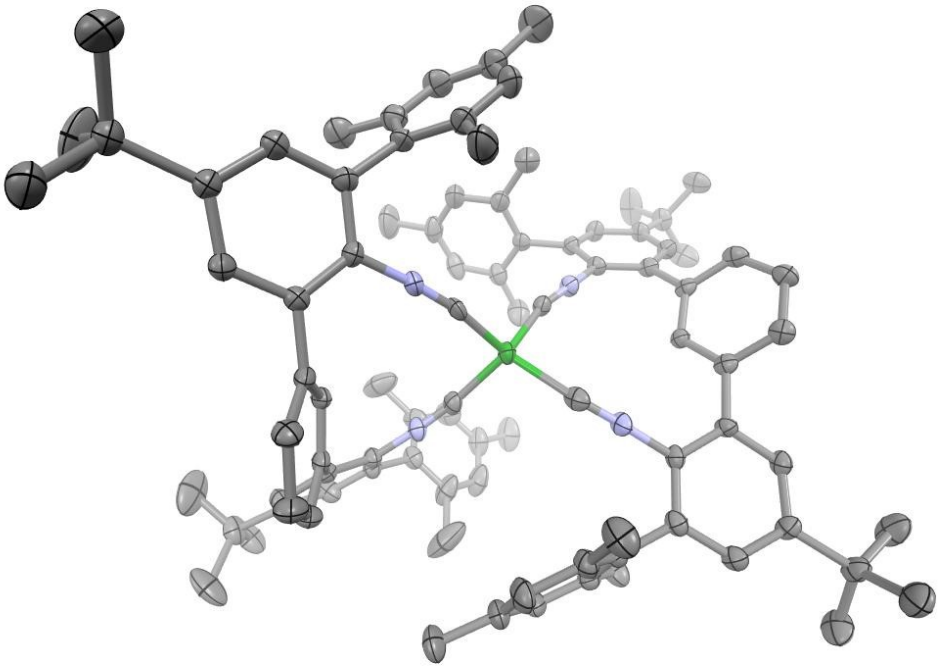

Figure S 18: X-ray crystal structure of ***[CuL^{CC}L^{CC}]$^{+}$****. Ellipsoids are drawn at 50% probability. Hydrogen atoms and counterions are omitted for clarity. Depth cueing has been applied to enhance structural visualization. Ellipsoids are drawn at 50% probability. Hydrogen atoms and counterions are omitted for clarity. Depth cueing has been applied to enhance structural visualization.*

Table S8: Selected bond length and angle of the four copper(I) complexes. The geometry index was calculated with the formula from the literature.[6]

Compound	**$[CuL^{NN}L^{PP}]^+$**	**$[CuL^{CC}L^{PP}]^+$**	**$[CuL^{CC}L^{NN}]^+$**	**$[CuL^{CC}L^{CC}]^+$**
bond length (Å)				
$Cu\text{-}C_1$ | $Cu\text{-}C_2$		1.938(8) | 1.947(9)	1.937(6) | 1.873(5)	1.931(5) | 1.956(5)
$Cu\text{-}C_3$ | $Cu\text{-}C_4$				1.952(5) | 1.942(5)
$Cu\text{-}P_1$ | $Cu\text{-}P_2$	2.2863(9) | 2.4265(9)	2.305(2) | 2.294(2)		
$Cu\text{-}N_1$ | $Cu\text{-}N_2$	2.164(3) | 2.192(2)		2.083(4) | 2.090(4)	
angle (°)				
$C_1\text{-}Cu\text{-}C_2$		94.9(3)	100.9(2)	99.5(2)
$C_3\text{-}Cu\text{-}C_4$				97.0(2)
$P_1\text{-}Cu\text{-}P_2$	112.09(3)	111.46(8)		
$N_1\text{-}Cu\text{-}N_2$	77.0(1)		80.7(2)	
$C_1\text{-}Cu\text{-}C_3/N_1/P_1$		111.8(2)	105.3(2)	122.4(2)
$C_1\text{-}Cu\text{-}C_4/N_2/P_2$		112.6(2)	103.8(2)	112.0(2)
$C_2\text{-}Cu\text{-}C_3/N_1/P_1$		109.1(2)	125.0(2)	108.5(2)
$C_2\text{-}Cu\text{-}C_4/N_2/P_2$		116.1(2)	137.3(2)	118.9(2)
$P_1\text{-}Cu\text{-}N_1$	130.25(7)			
$P_1\text{-}Cu\text{-}N_2$	130.41(7)			
$P_2\text{-}Cu\text{-}N_1$	100.13(7)			
$P_2\text{-}Cu\text{-}N_2$	98.75(7)			
geometry index				
τ_4	0.70	0.94	0.69	0.84

$$\tau_4 = \frac{360\,^\circ - (\alpha + \beta)}{141\,^\circ}$$

The geometry index (τ_4) of all four complexes was calculated using the formula developed in the literature[8], where α and β correspond to the two largest ligand-metal-ligand bond angles around the copper center. A τ_4 value of one indicates an ideal tetrahedral geometry, while a value of zero corresponds to a perfect square-planar geometry. **$[CuL^{CC}L^{PP}]^+$** exhibits a geometry close to tetrahedral (τ_4 = 0.94), **$[CuL^{NN}L^{PP}]^+$** and **$[CuL^{CC}L^{NN}]^+$**, with τ_4 values of 0.70 and 0.69, are strongly distorted towards a seesaw geometry. **$[CuL^{CC}L^{CC}]^+$** displays an intermediate value (τ_4 = 0.84) corresponding to a geometry best described as trigonal pyramidal.

Table S9: Geometry index (τ_4) for selected tetrahedral Cu(I) complexes calculated from the two largest ligand-metal-ligand bond angles (α and β). Abbreviations are as follows: phen = 1,10-phenanthroline; dmp = 2,9-dimethyl-1,10-phenanthroline; binc = bis(2-isocyanophenyl) phenylphosphonate

	α / °	β / °	τ_4
$[Cu(phen)_2]^+$ [a]	147.45 (N-Cu-N)	147.45 (N-Cu-N)	0.46
$[Cu(xantphos)(phen)]^+$ [b]	129.87 (C-Cu-P)	115.00 (C-Cu-P)	0.82
$[Cu(dmp)(binc)]^+$ [c]	124.65 (C-Cu-N)	124.63 (C-Cu-N)	0.79

The crystal structures from where the data were extrapolated are: [a] ref [9], [b] ref [10], [c] ref [11].

8 Temperature dependent NMR study of $[CuL^{CC}L^{PP}]^+$

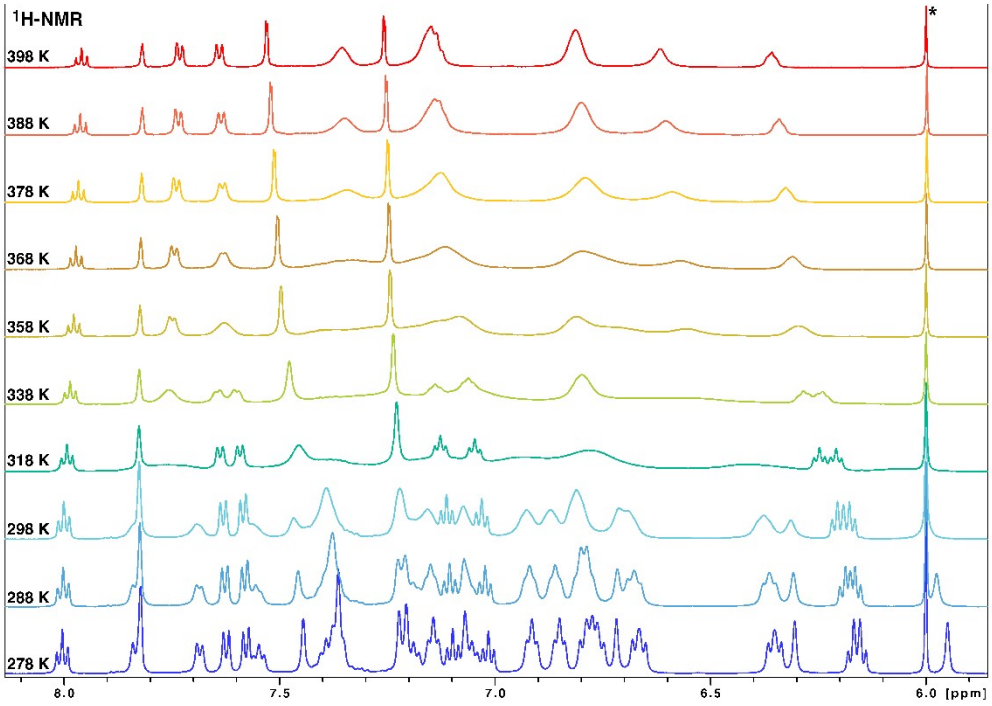

Figure S19: Stacked ^{1}H-NMR spectra (600 MHz) showing the aromatic region (5.9 – 8.1 ppm) of ***$[CuL^{CC}L^{PP}]^+$*** *in $C_2D_2Cl_4$ (*) recorded at different temperatures (278 - 398 K) as indicated in the figure.*

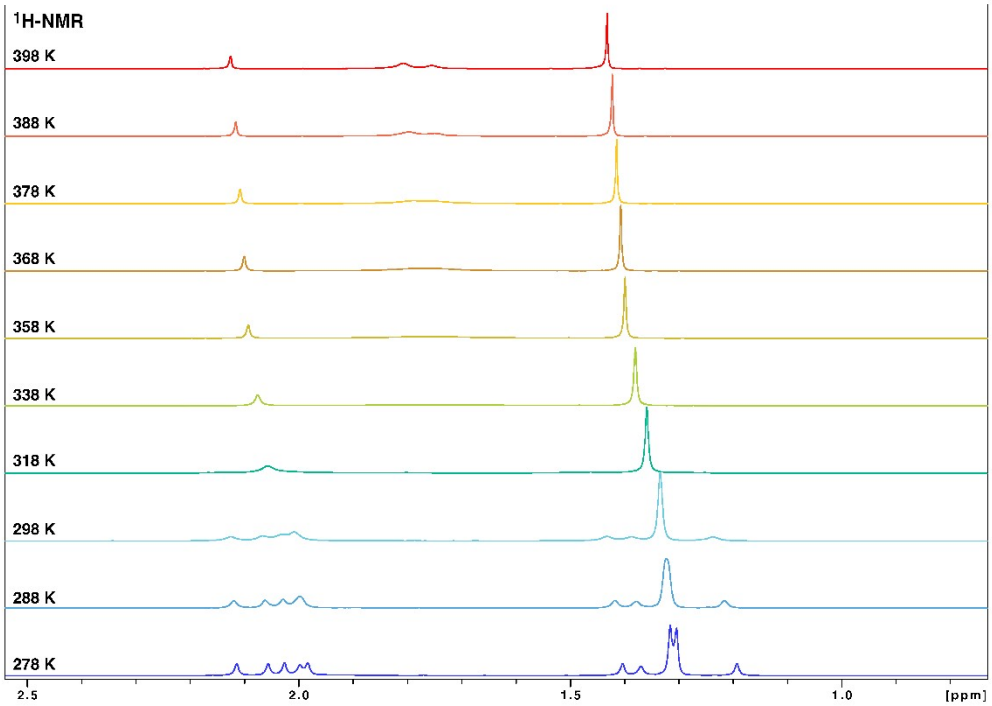

Figure S20: Stacked ^{1}H-NMR spectra (600 MHz) showing the aliphatic region (0.8 - 2.5 ppm) of ***$[CuL^{CC}L^{PP}]^+$*** *in $C_2D_2Cl_4$ recorded at different temperatures (278 - 398 K) as indicated in the figure.*

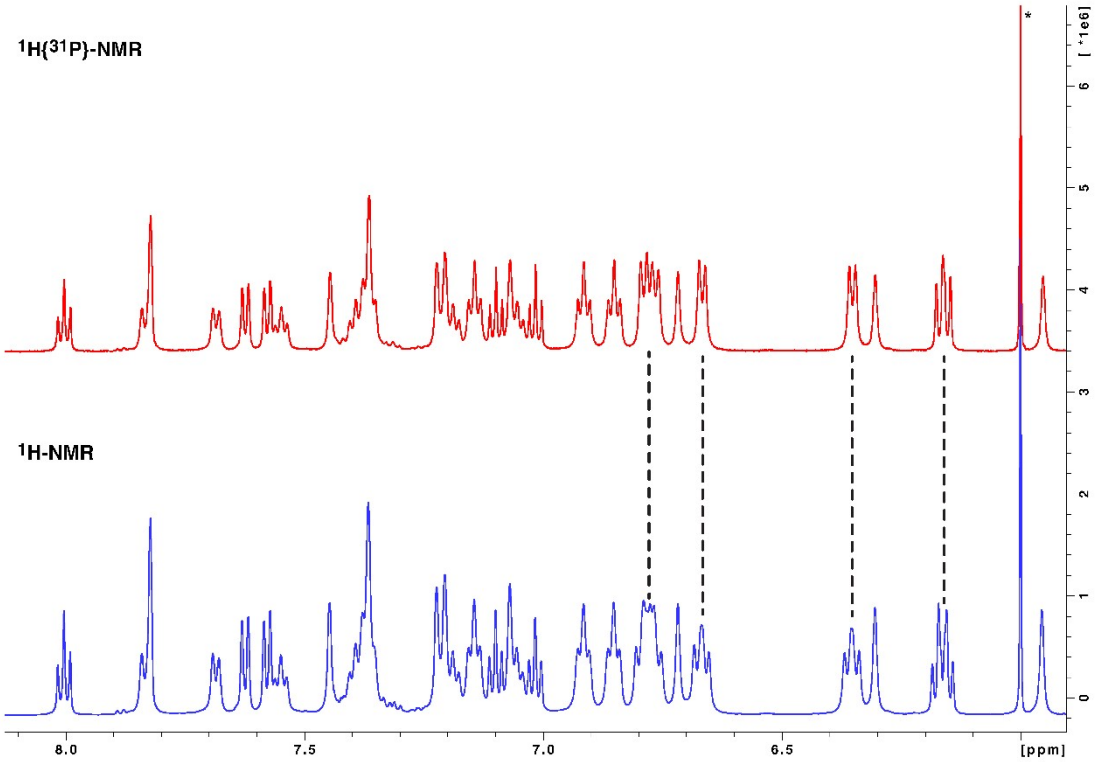

Figure S21: Stacked ^{1}H-NMR (bottom) and ^{1}H{^{31}P}-NMR (top) spectra (600 MHz) showing the aromatic region (5.9 – 8.1 ppm) of ***[CuL^{CC}L^{PP}]$^+$*** *in $C_2D_2Cl_4$ (*) recorded at 278 K. Signals marked with dotted lines indicate coupling to the phosphorus atom.*

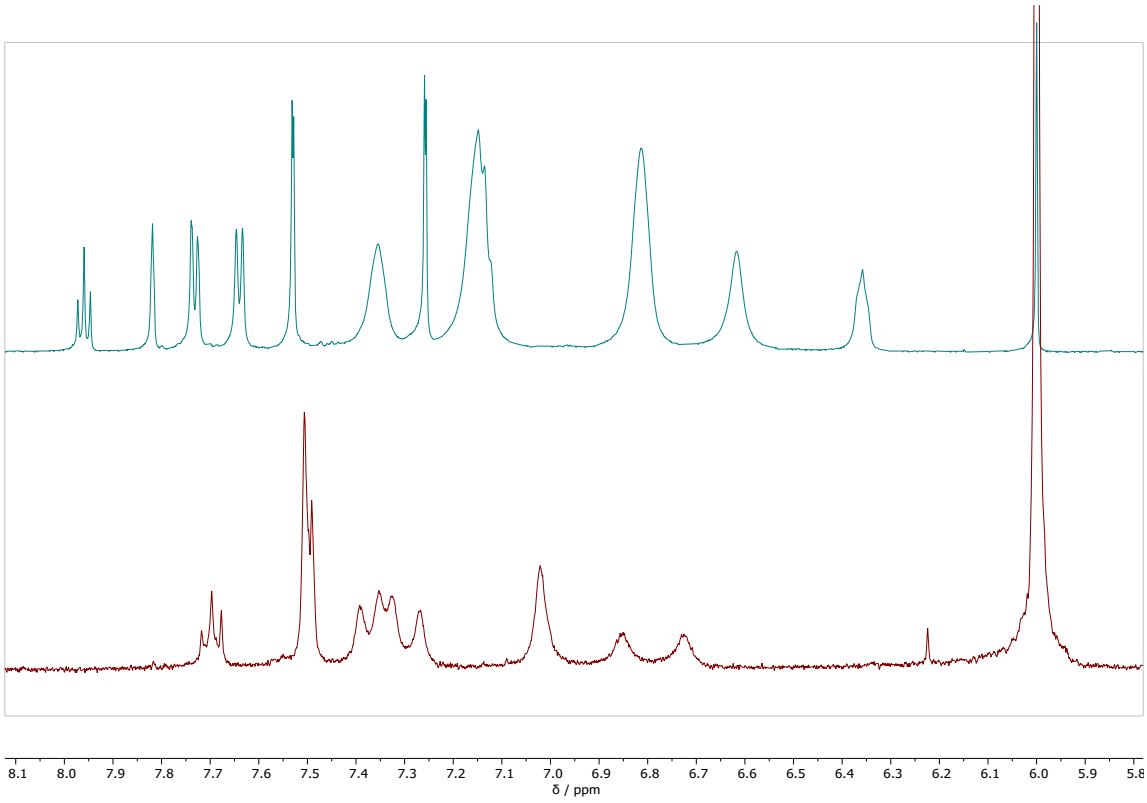

Figure S22: Stacked ^{1}H-NMR spectra of ***[CuL^{CC}L^{PP}]$^+$*** *(600 MHz, 398 K) (top) and* ***[CuL^{CC}L^{PP}]$^+$*** *(400 MHz, 298 K) (bottom) showing the aromatic region (5.8 – 8.1 ppm) in $C_2D_2Cl_4$.*

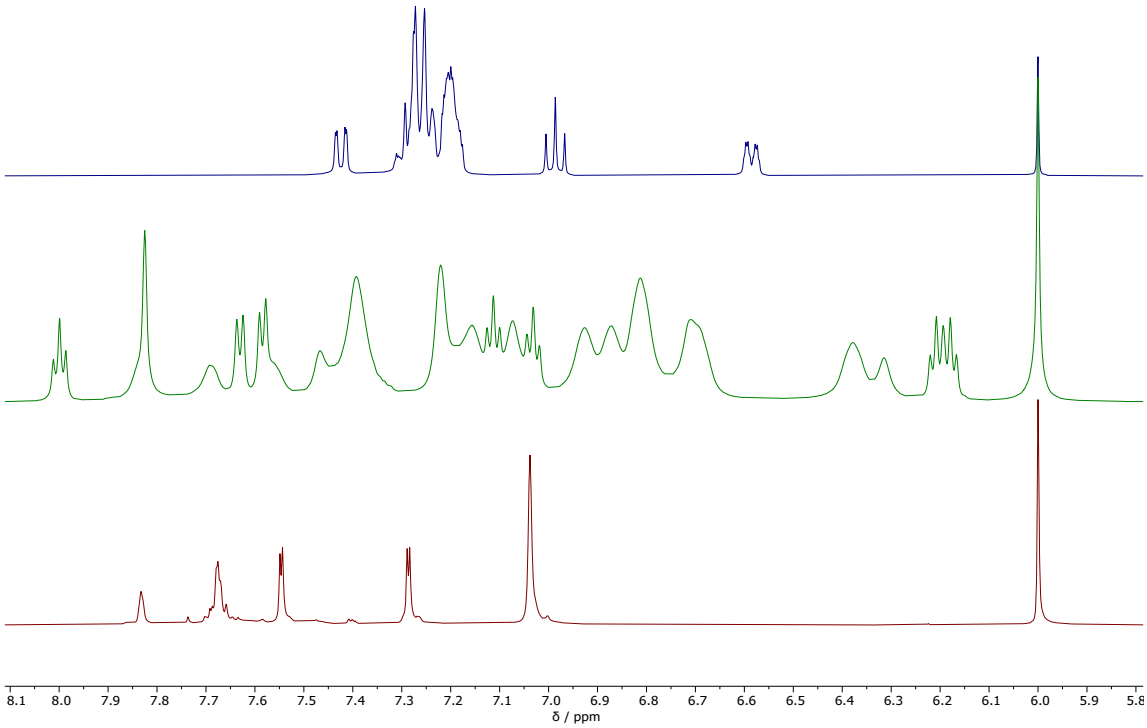

*Figure S23: Stacked ^{1}H-NMR spectra of **L^{PP}** (400 MHz, 298 K), **[CuL^{CC}L^{PP}]$^{+}$** (600 MHz, 298 K) (middle) and **L^{CC}** (400 MHz, 298 K) (bottom) showing the aromatic region (5.8 – 8.1 ppm) in $C_2D_2Cl_4$.*

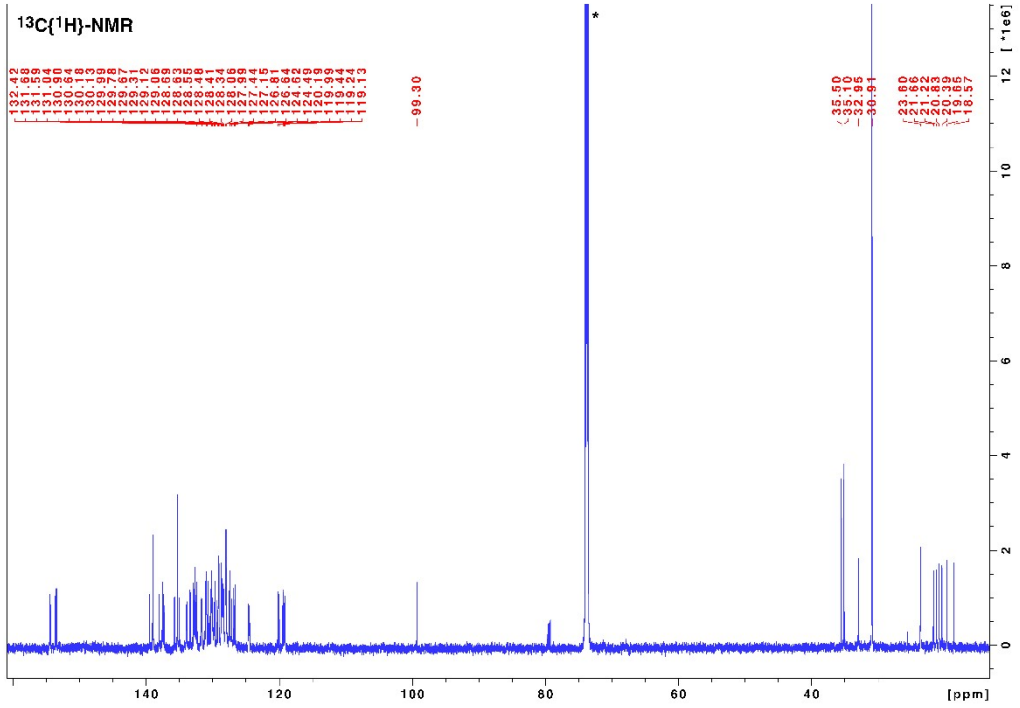

*Figure S24: ^{13}C{^{1}H}-NMR spectrum (151 MHz, 278 K) of **[CuL^{CC}L^{PP}]$^{+}$** in $C_2D_2Cl_4$ (*).*

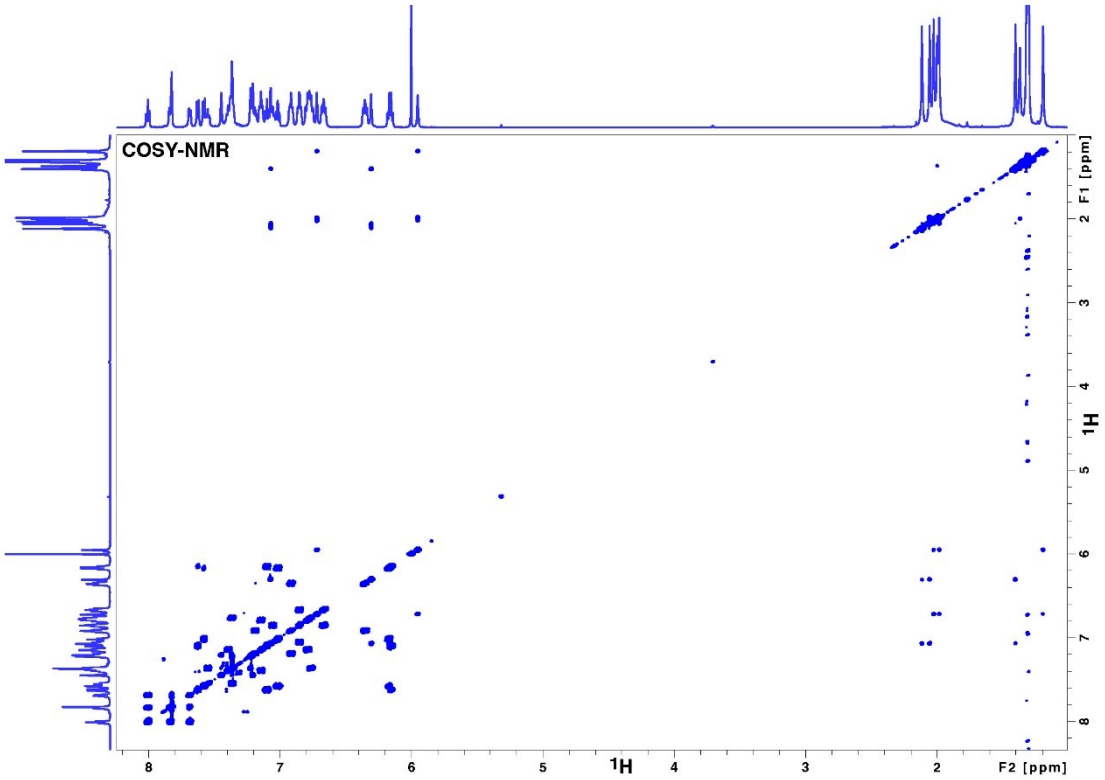

Figure S25: $^{1}H,^{1}H$-COSY spectrum (600 MHz, 600 MHz, 278 K) of ***[CuL^{CC}L^{PP}]$^{+}$*** *in $C_2D_2Cl_4$.*

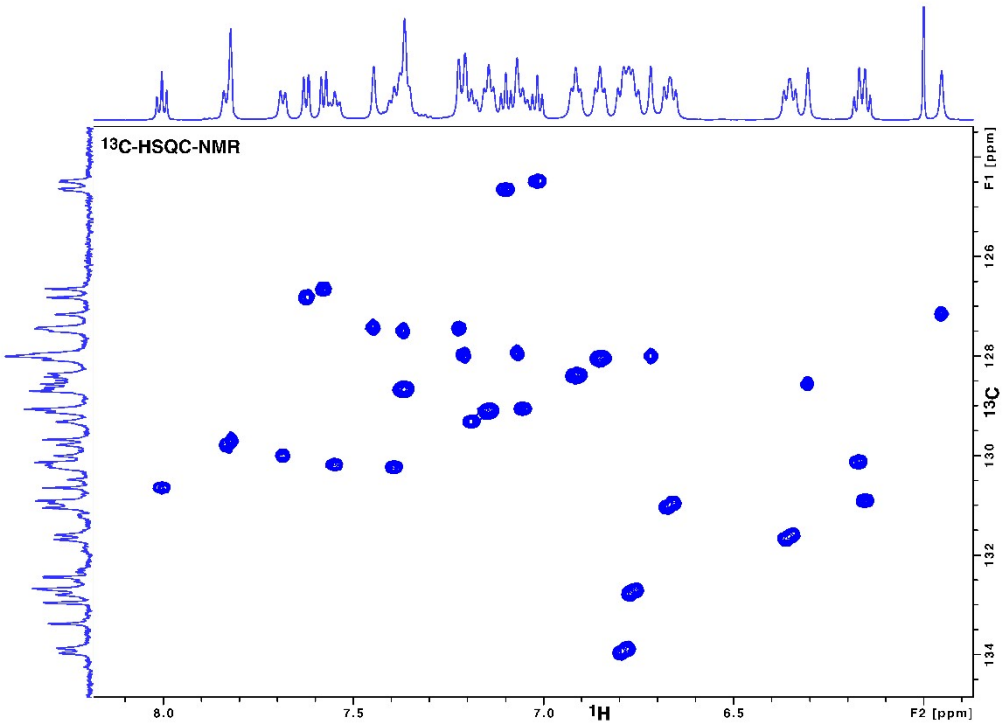

Figure S26: $^{1}H,^{13}C$-HSQC spectrum (600 MHz, 151 MHz, 278 K) of ***[CuL^{CC}L^{PP}]$^{+}$*** *in $C_2D_2Cl_4$.*

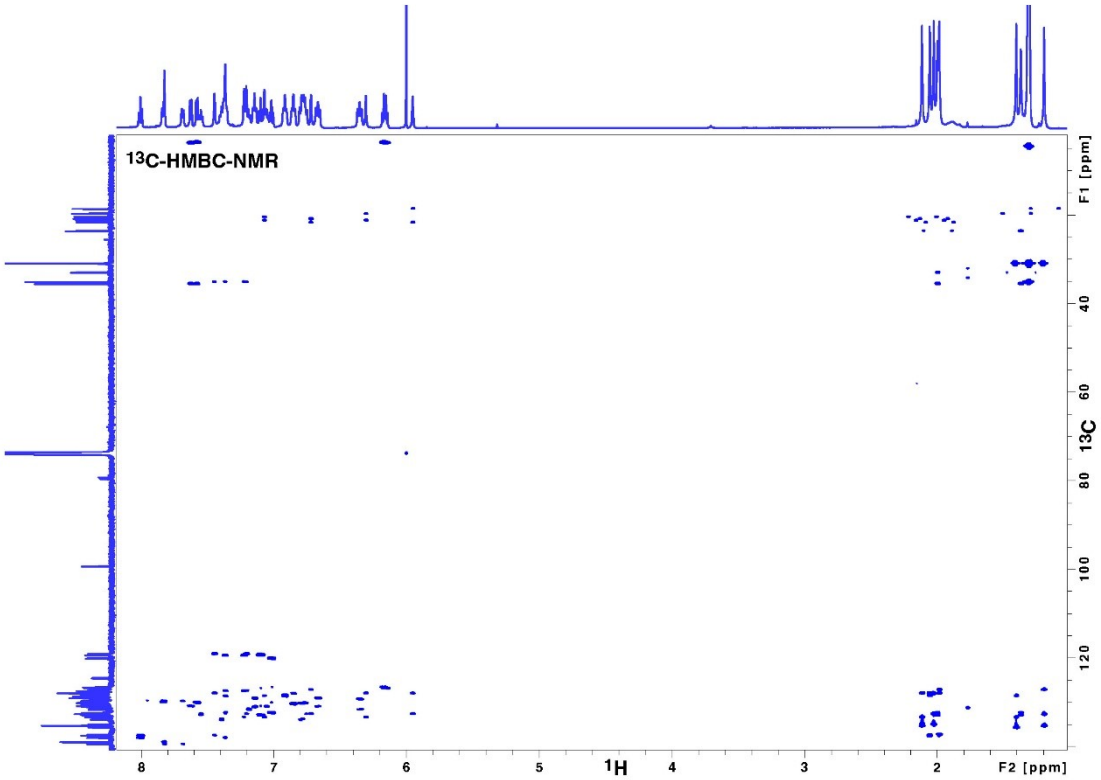

Figure S27: $^{1}H,^{13}C$-HMBC spectrum (600 MHz, 151 MHz, 278 K) of ***[CuL^{CC}L^{PP}]$^{+}$*** *in $C_2D_2Cl_4$.*

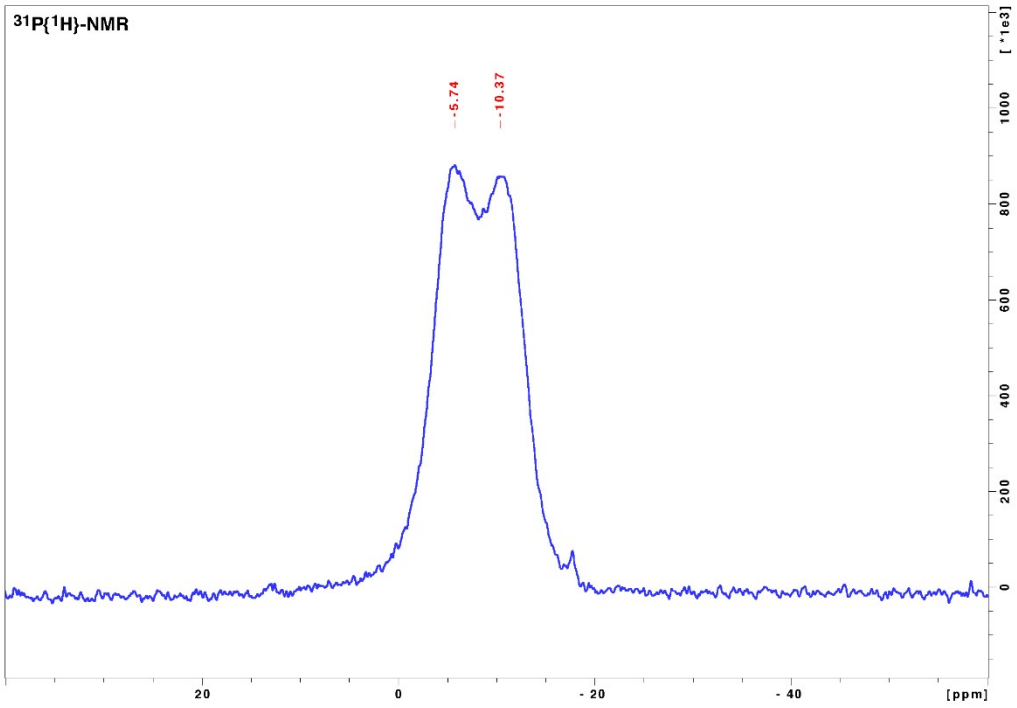

Figure S28: $^{31}P\{^{1}H\}$-NMR spectrum (243 MHz, 278 K) of ***[CuL^{NN}L^{PP}]$^{+}$*** *in $C_2D_2Cl_4$.*

9 NMR spectra

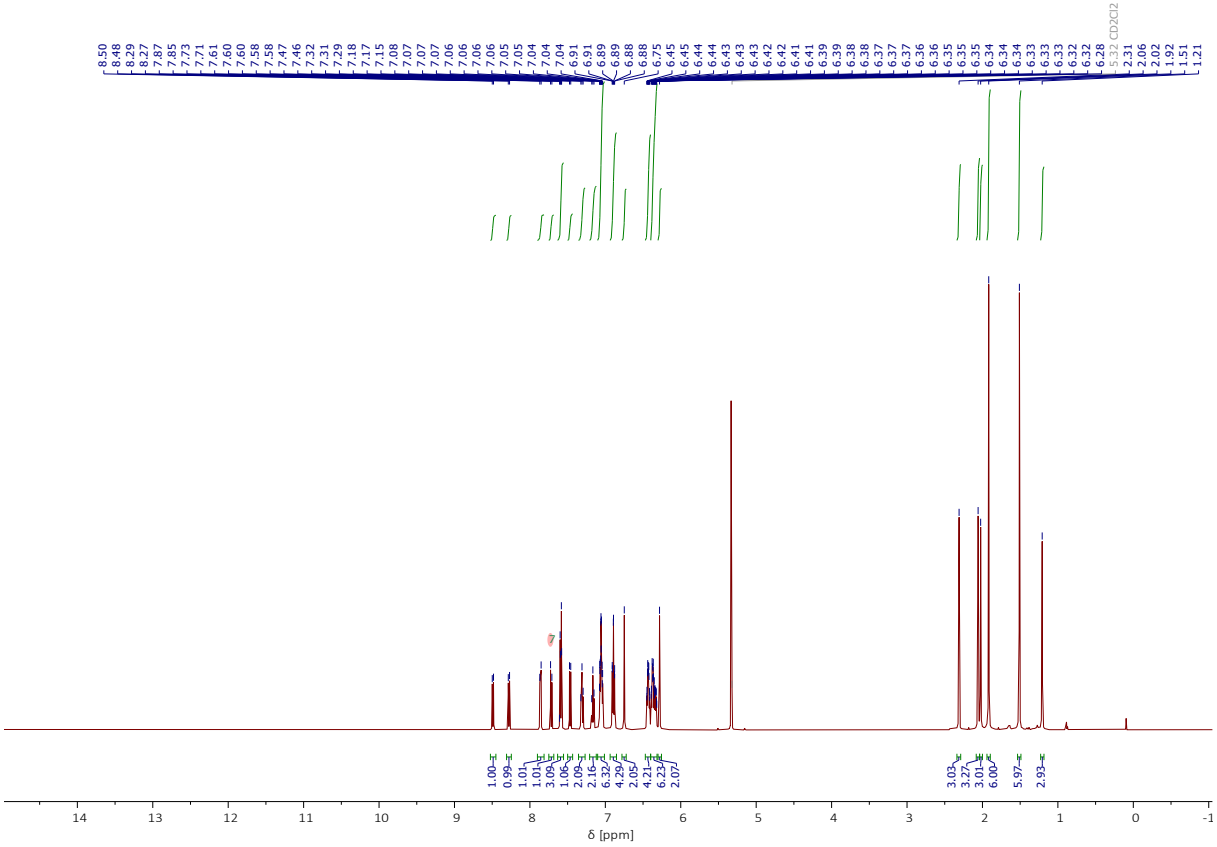

*Figure S29: ^{1}H-NMR spectrum (500 MHz, 298 K) of **[CuL^{NN}L^{PP}]$^{+}$** in CD_2Cl_2.*

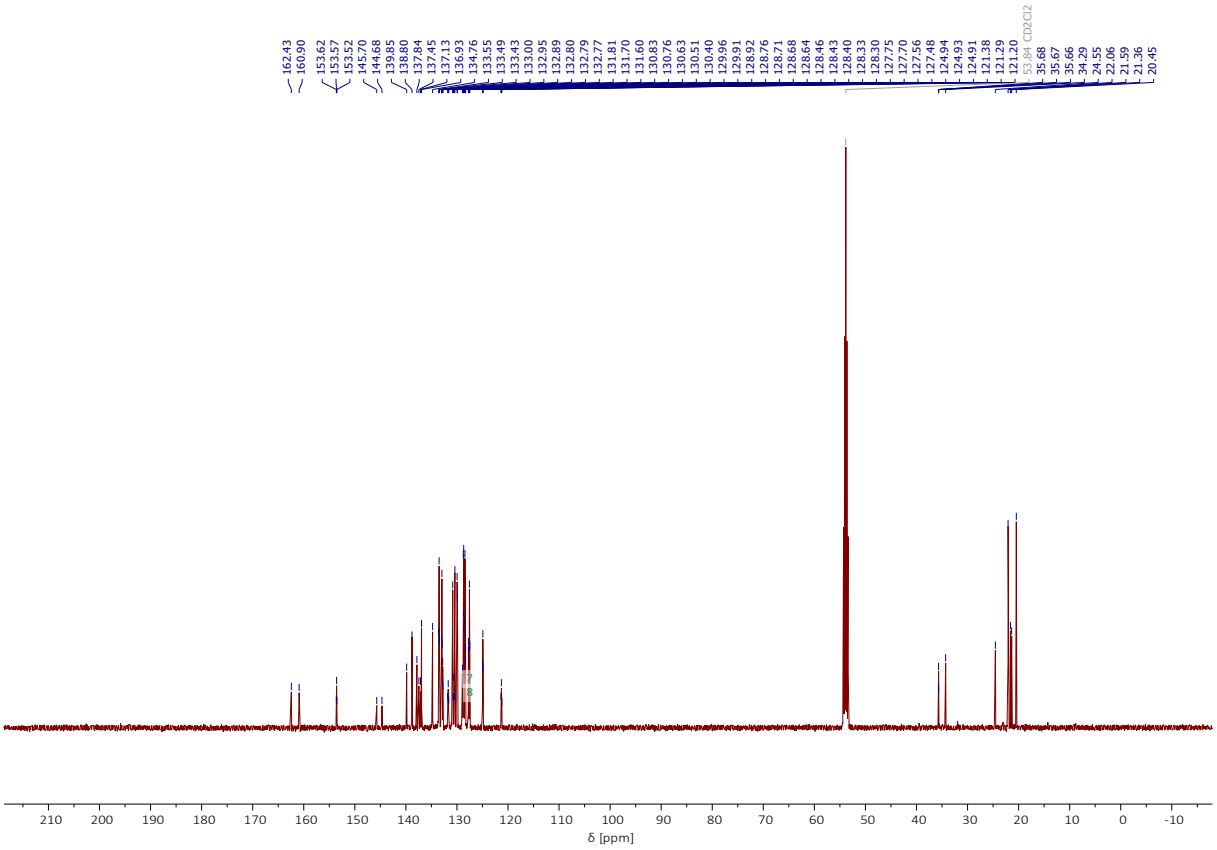

*Figure S30: ^{13}C{^{1}H}-NMR spectrum (126 MHz, 298 K) of **[CuL^{NN}L^{PP}]$^{+}$** in CD_2Cl_2.*

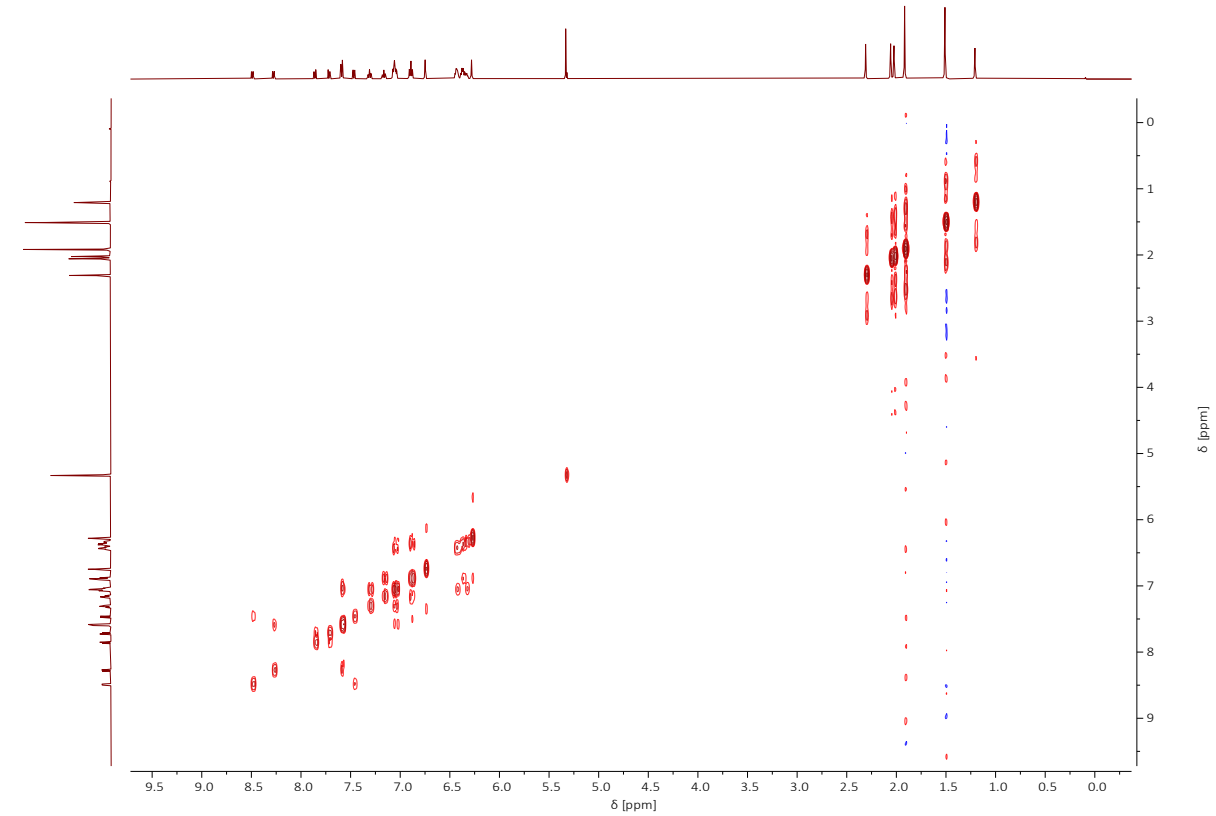

Figure S31: ^{1}H, ^{1}H-COSY spectrum (500 MHz, 500 MHz, 298 K) of ***[CuL^{NN}L^{PP}]$^{+}$*** *in CD_2Cl_2.*

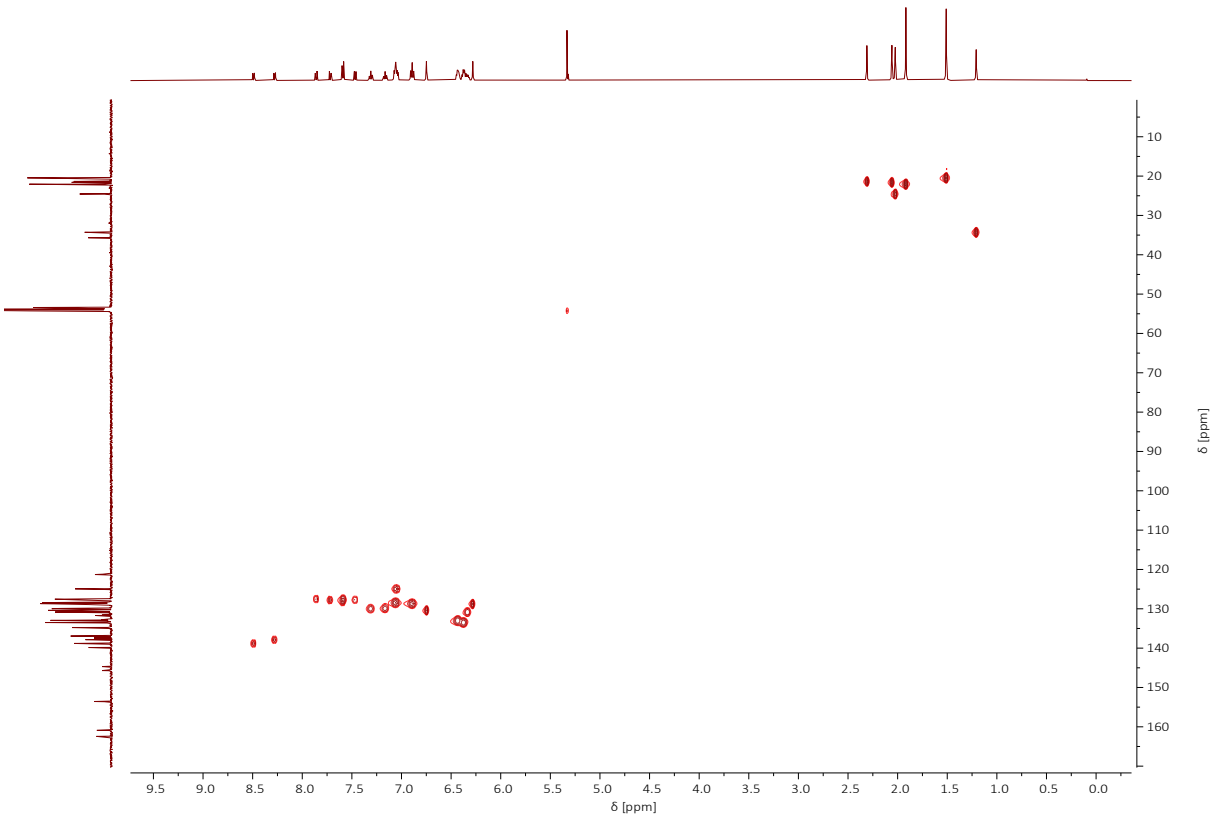

Figure S32: ^{1}H,^{13}C-HMQC spectrum (500 MHz, 126 MHz, 298 K) of ***[CuL^{NN}L^{PP}]$^{+}$*** *in CD_2Cl_2.*

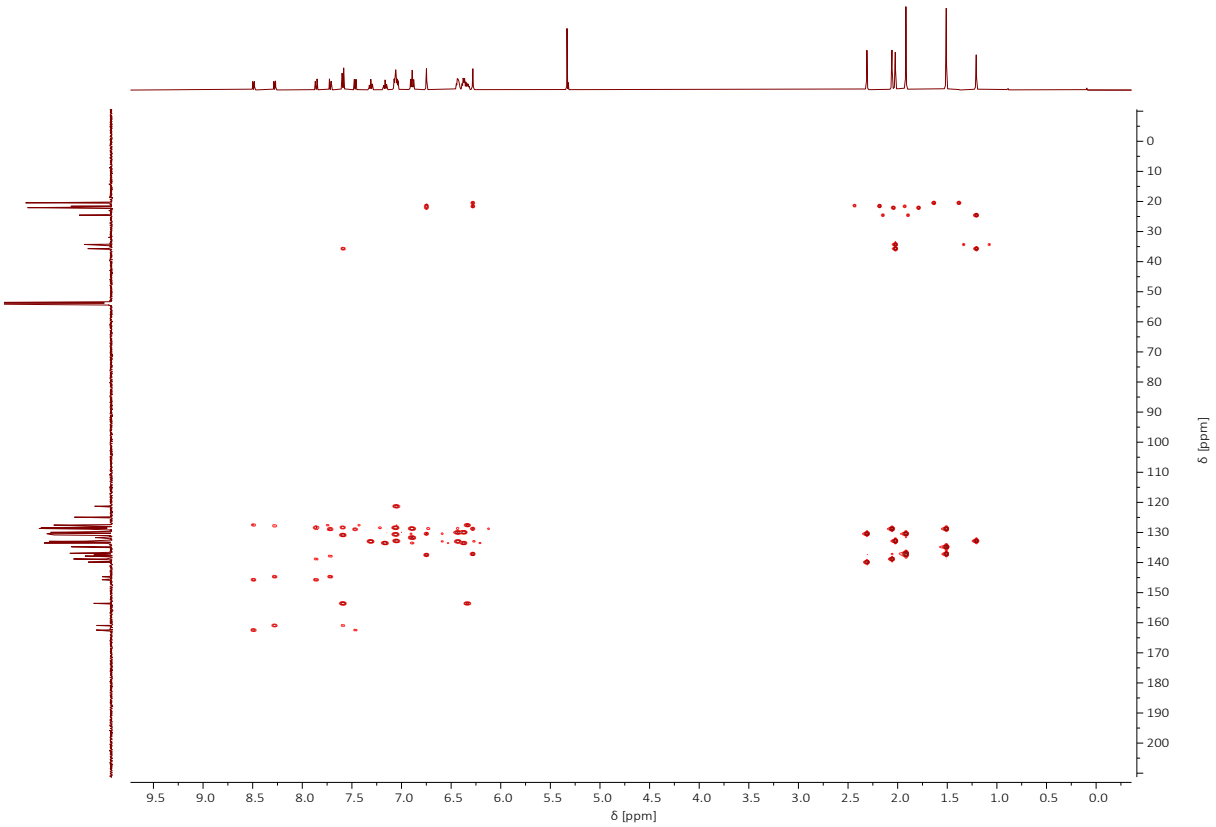

*Figure S33: $^{1}H,^{13}C$-HMBC spectrum (500 MHz, 126 MHz, 298 K) of **[CuL^{NN}L^{PP}]$^{+}$** in CD_2Cl_2.*

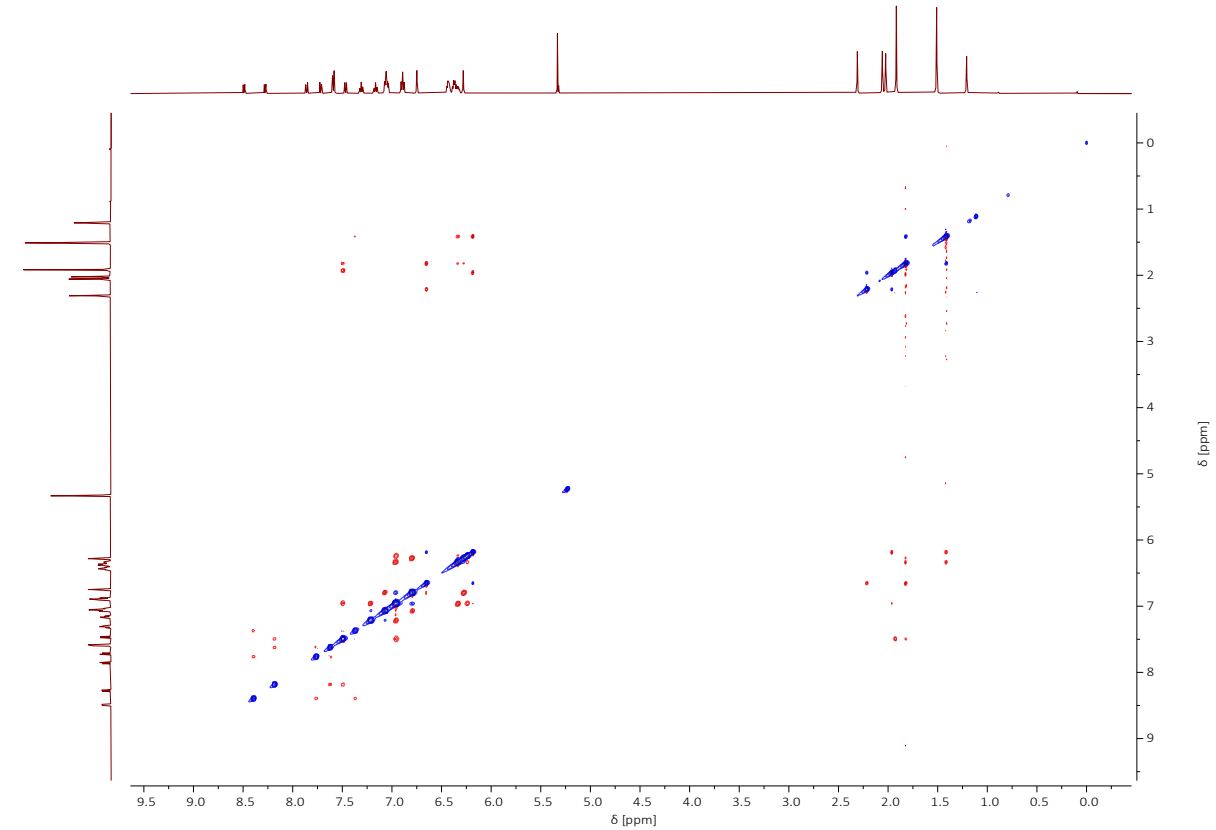

*Figure S34: $^{1}H,^{13}C$-NOESY spectrum (500 MHz, 126 MHz, 298 K) of **[CuL^{NN}L^{PP}]$^{+}$** in CD_2Cl_2.*

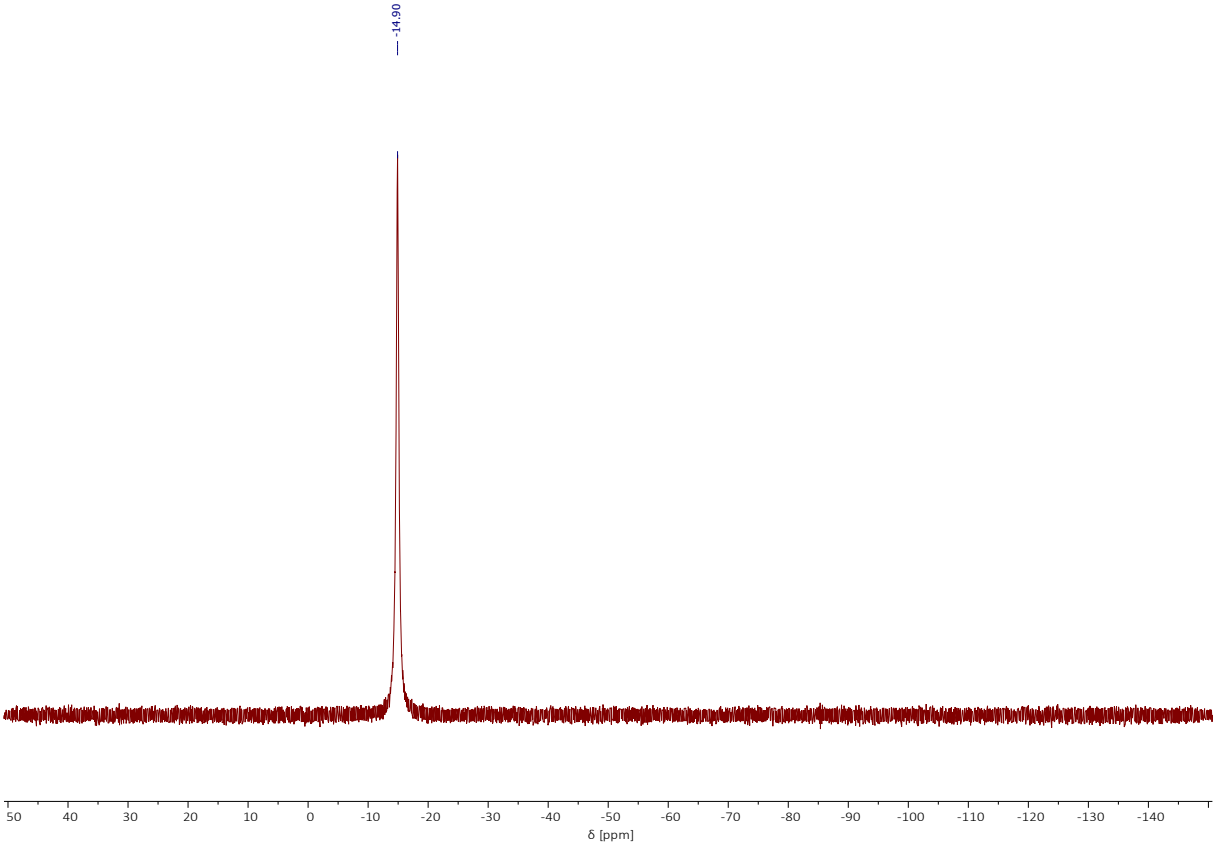

*Figure S35: $^{31}P\{^{1}H\}$-NMR spectrum (202 MHz, 298 K) of **$[CuL^{NN}L^{PP}]^{+}$** in CD_2Cl_2.*

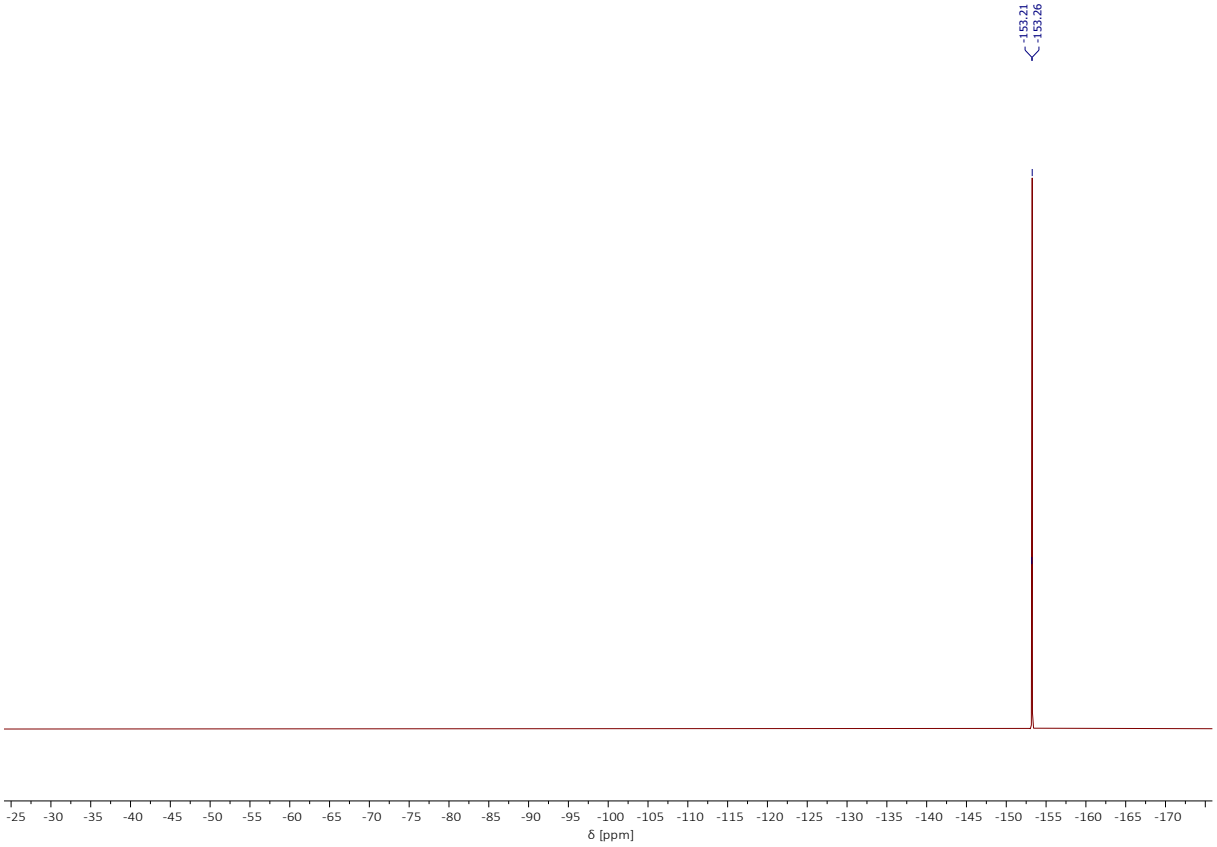

*Figure S36: $^{19}F\{^{1}H\}$-NMR spectrum (471 MHz, 298 K) of **$[CuL^{NN}L^{PP}]^{+}$** in CD_2Cl_2.*

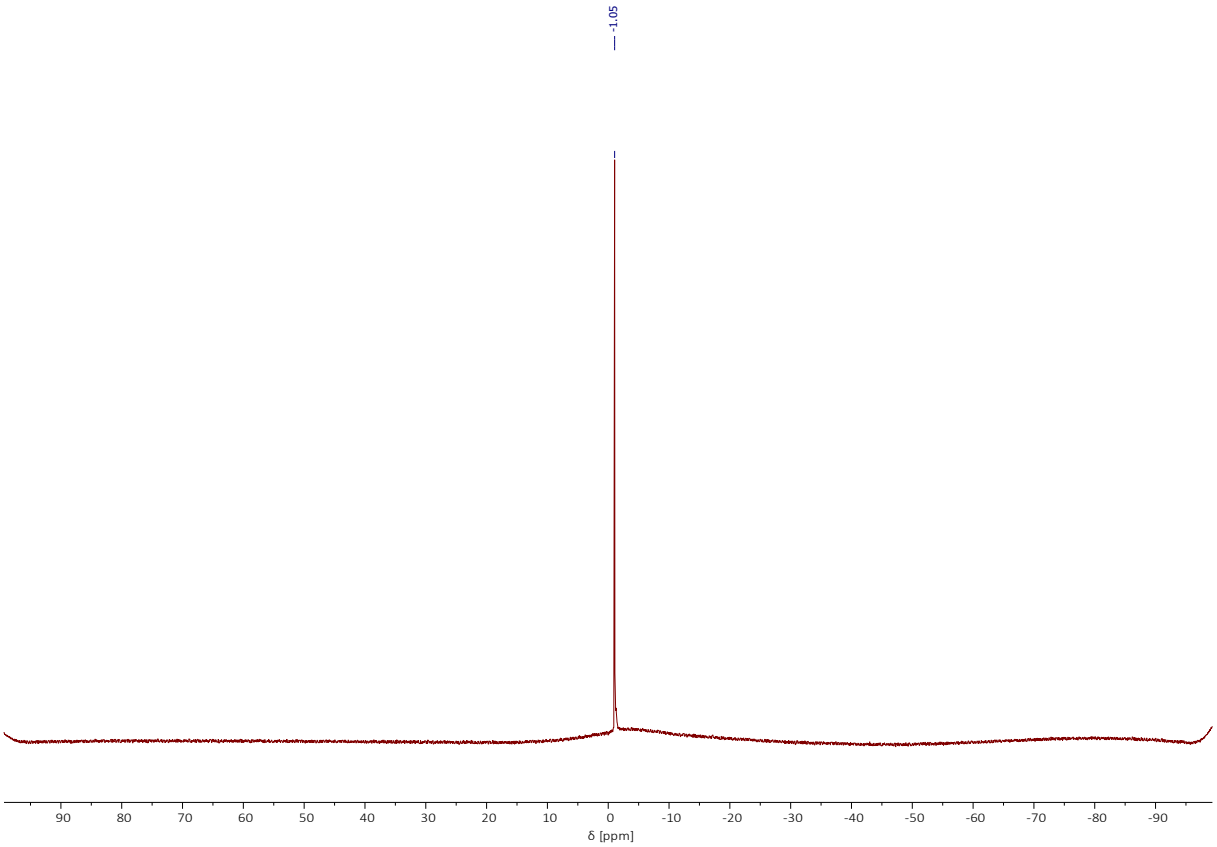

*Figure S37: ^{11}B-NMR spectrum (128 MHz, 298 K) of **[CuL^{NN}L^{PP}]$^{+}$** in CD_2Cl_2.*

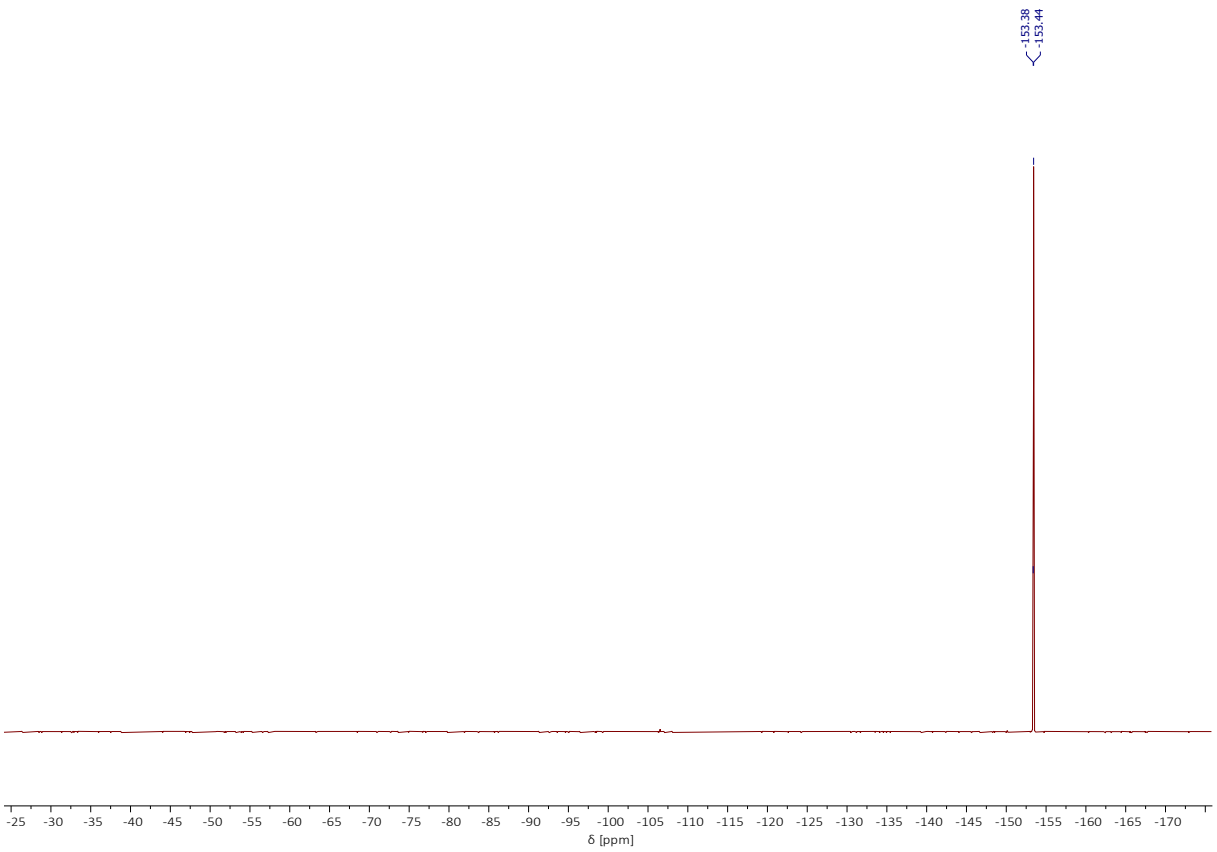

*Figure S38: ^{19}F{^{1}H}-NMR spectrum (471 MHz, 298 K) of **[CuL^{CC}L^{PP}]$^{+}$** in CD_2Cl_2.*

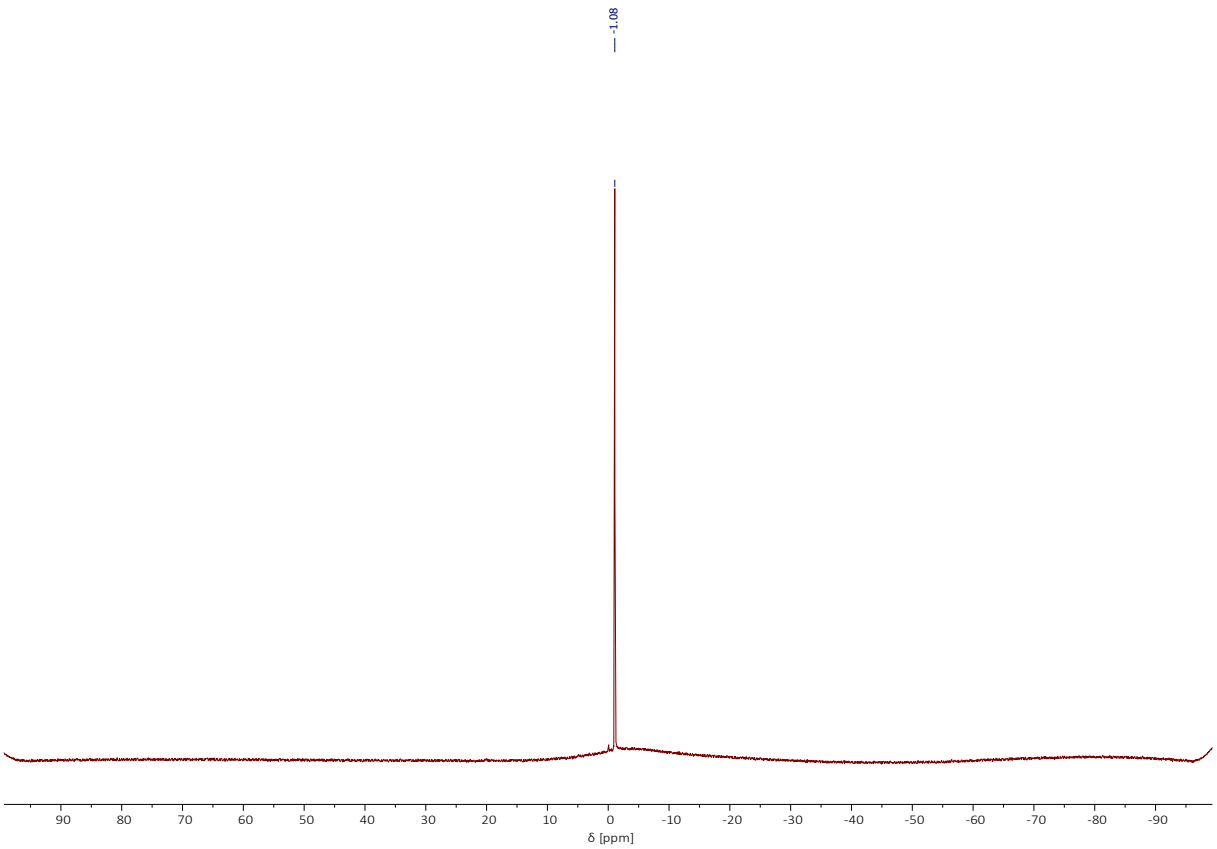

*Figure S39: ^{11}B-NMR spectrum (128 MHz, 298 K) of **[CuL^{CC}L^{PP}]$^{+}$** in CD_2Cl_2.*

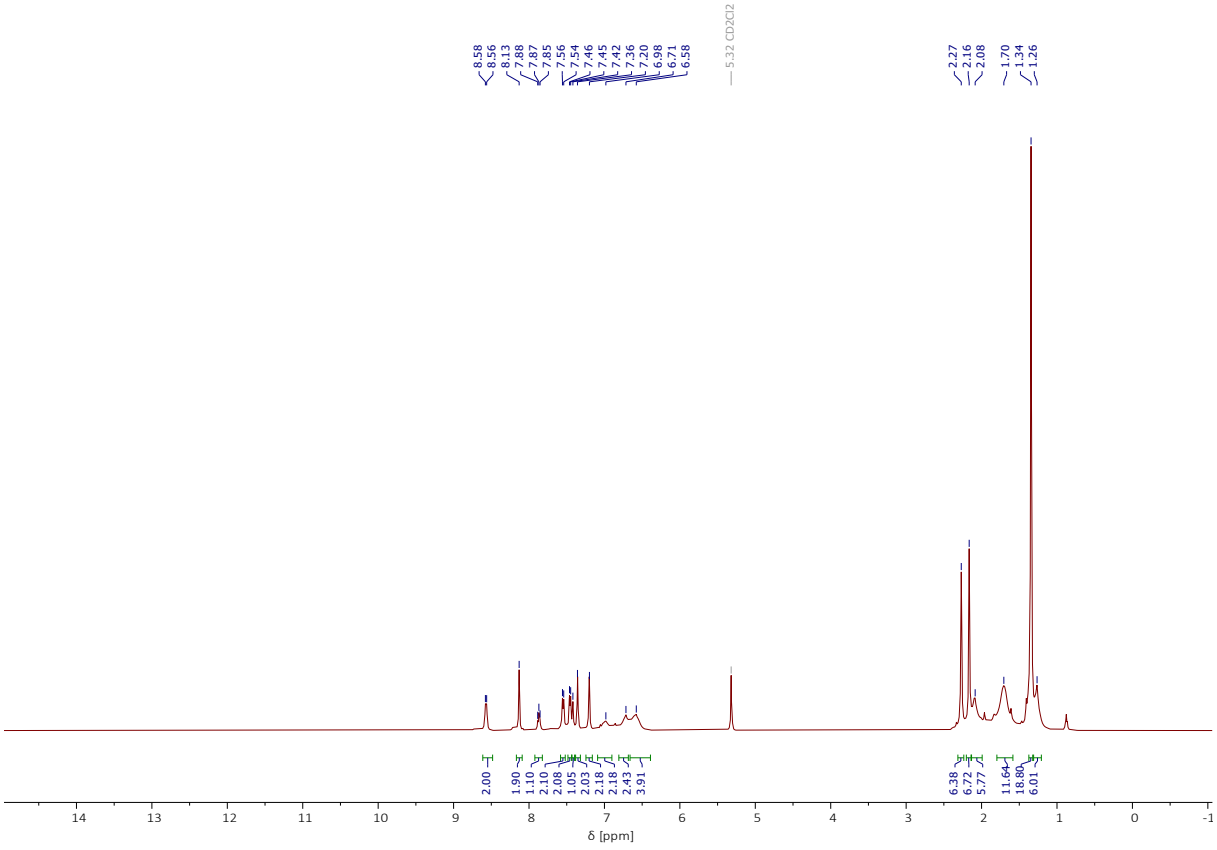

*Figure S40: ^{1}H-NMR spectrum (500 MHz, 298 K) of **[CuL^{CC}L^{NN}]$^{+}$** in CD_2Cl_2.*

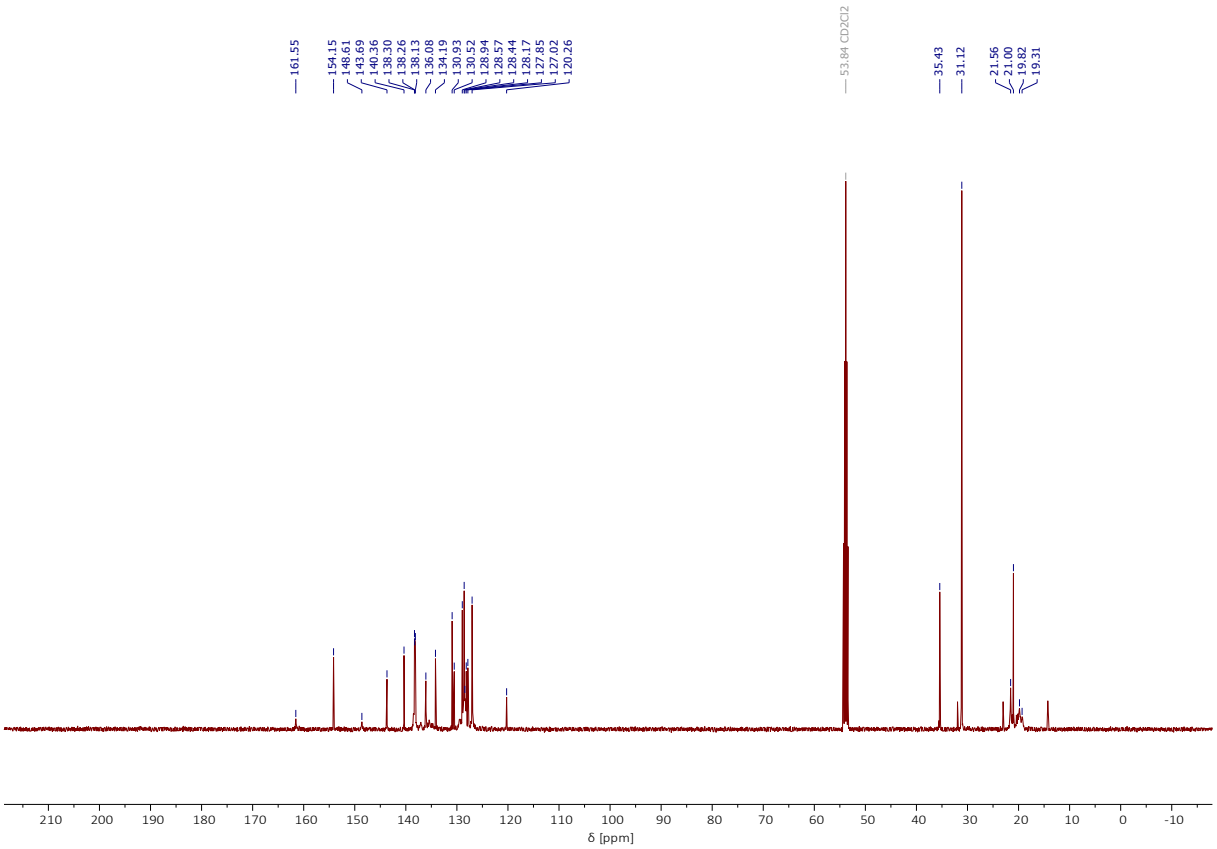

Figure S41: $^{13}C\{^{1}H\}$-NMR spectrum (126 MHz, 298 K) of ***[CuL^{CC}L^{NN}]$^{+}$*** *in CD_2Cl_2.*

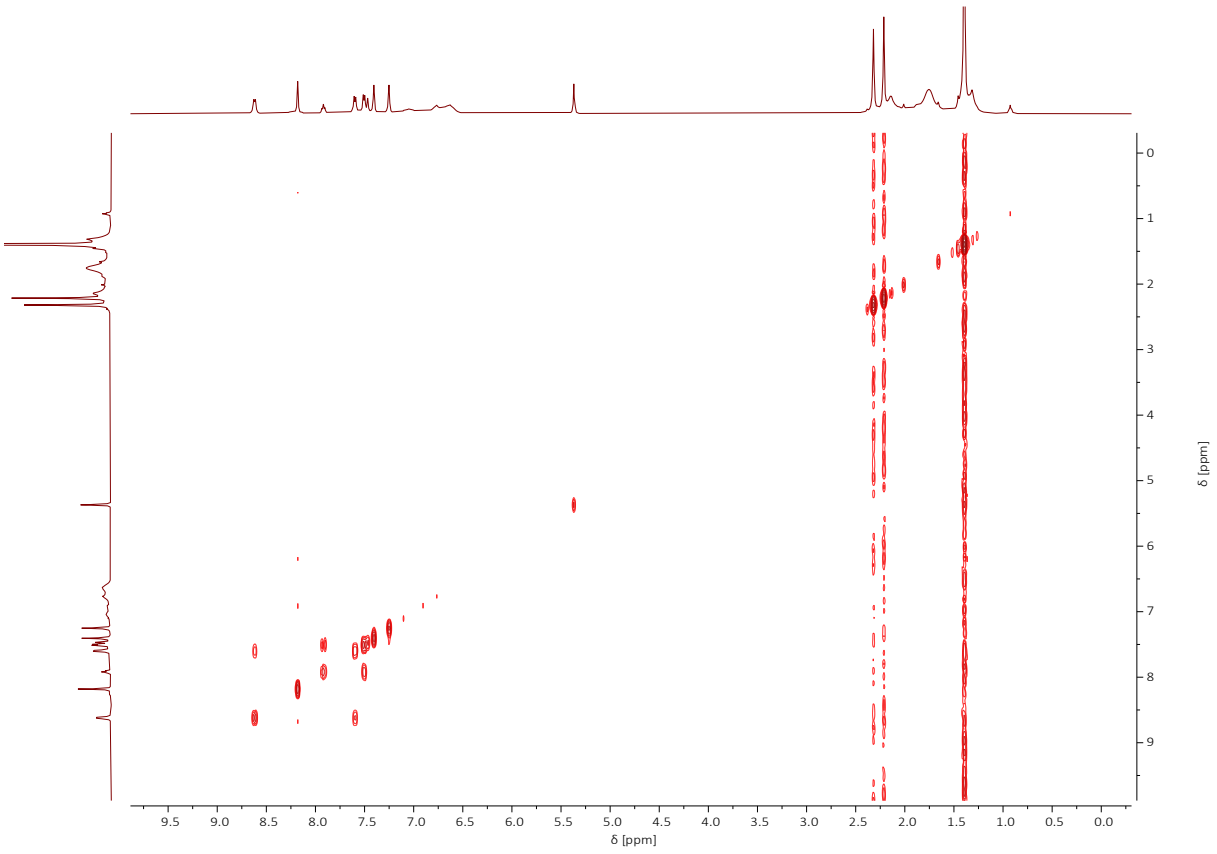

Figure S42: $^{1}H, ^{1}H$-COSY spectrum (500 MHz, 500 MHz, 298 K) of ***[CuL^{CC}L^{NN}]$^{+}$*** *in CD_2Cl_2.*

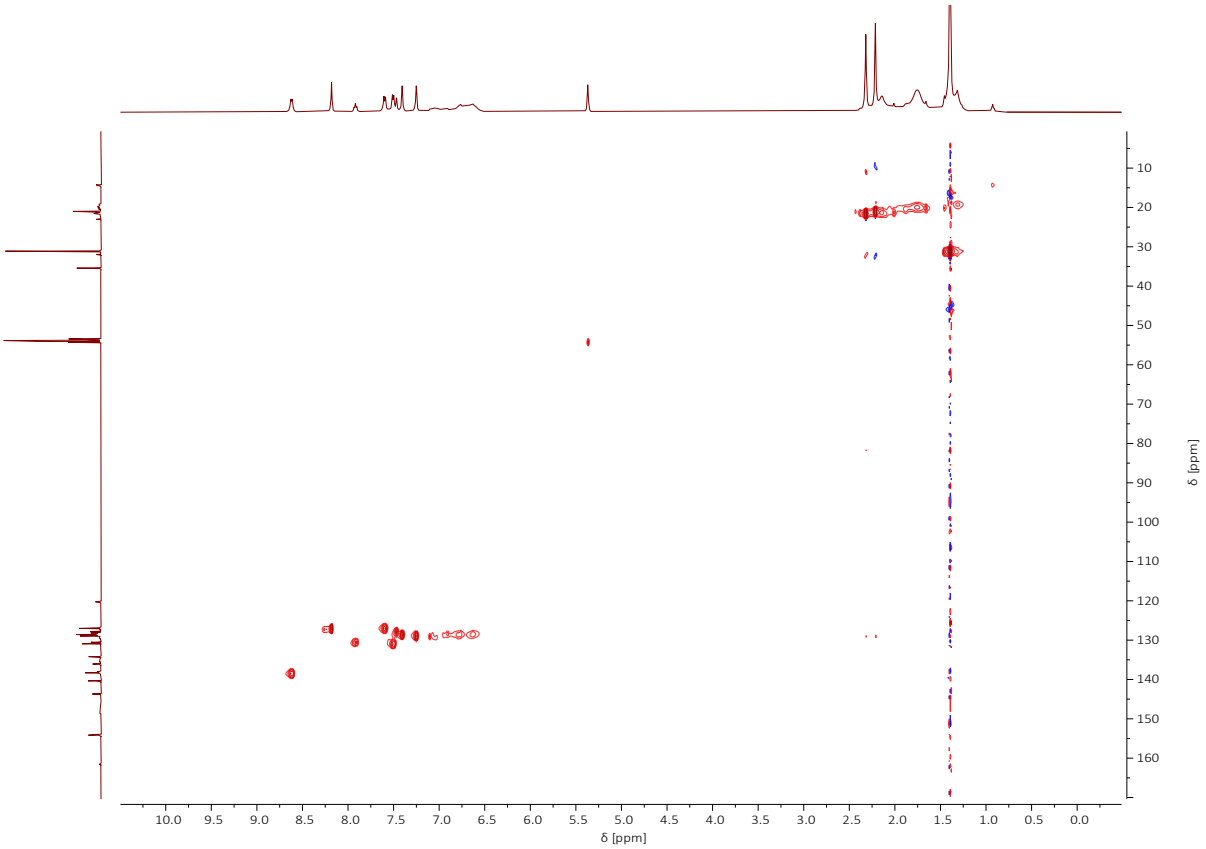

*Figure S43: $^{1}H,^{13}C$-HMQC spectrum (500 MHz, 126 MHz, 298 K) of **[CuL^{CC}L^{NN}]$^{+}$** in CD_2Cl_2.*

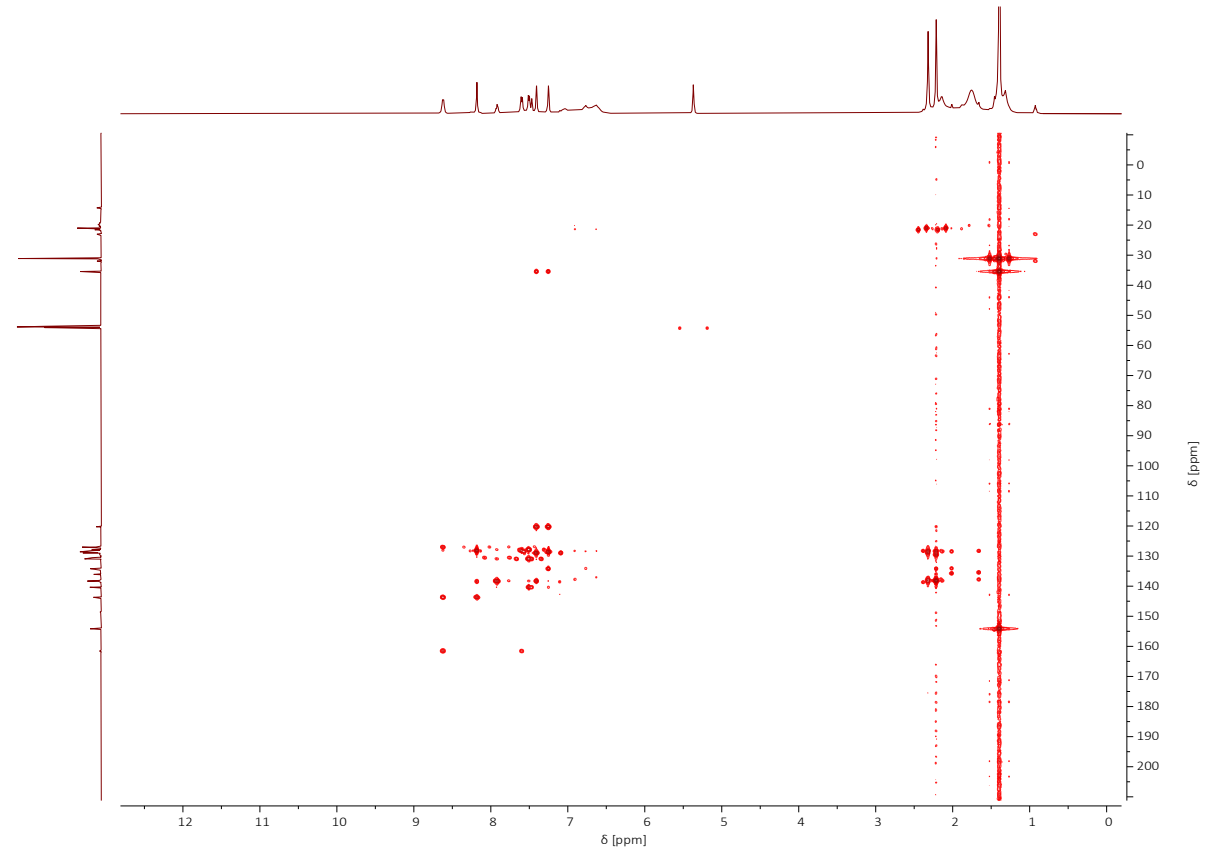

*Figure S44: $^{1}H,^{13}C$-HMBC spectrum (500 MHz, 126 MHz, 298 K) of **[CuL^{CC}L^{NN}]$^{+}$** in CD_2Cl_2.*

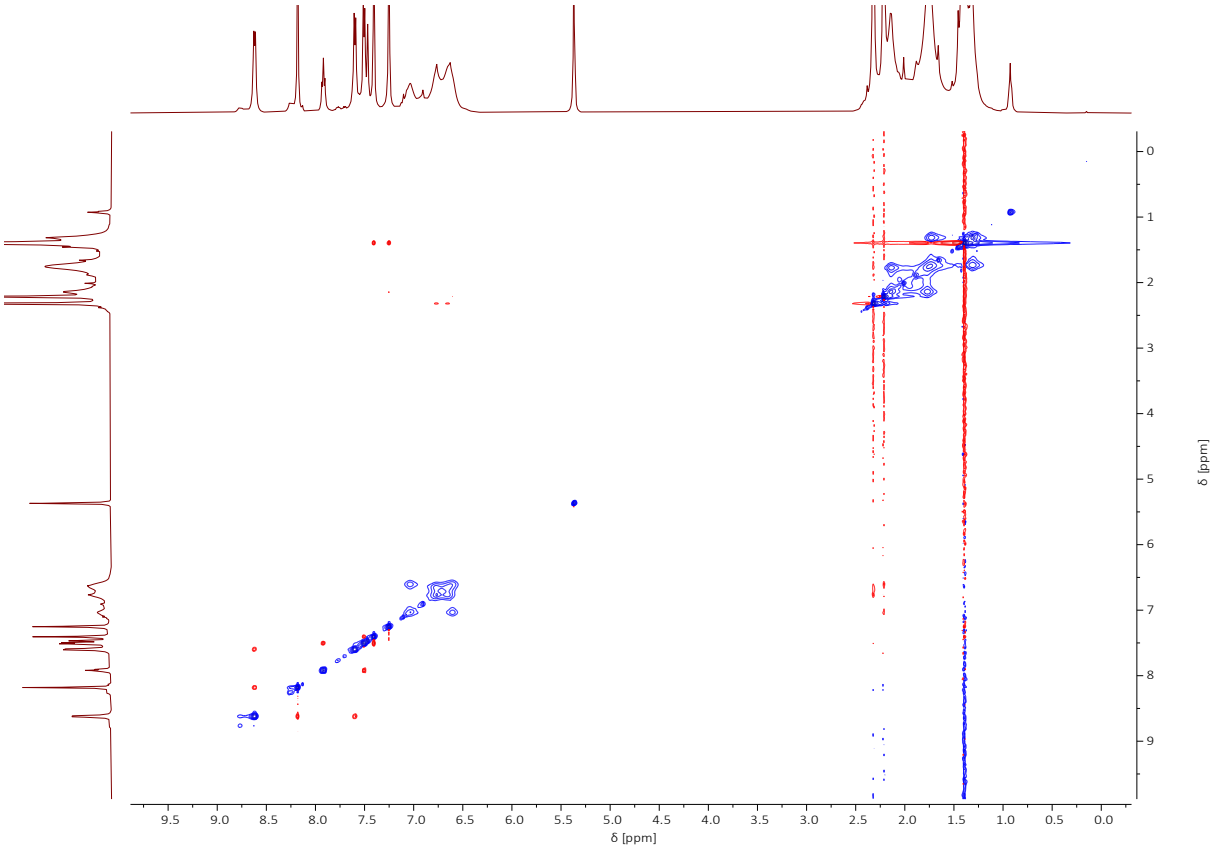

*Figure S45: $^{1}H,^{13}C$-NOESY spectrum (500 MHz, 126 MHz, 298 K) of **[CuL^{CC}L^{NN}]$^{+}$** in CD_2Cl_2.*

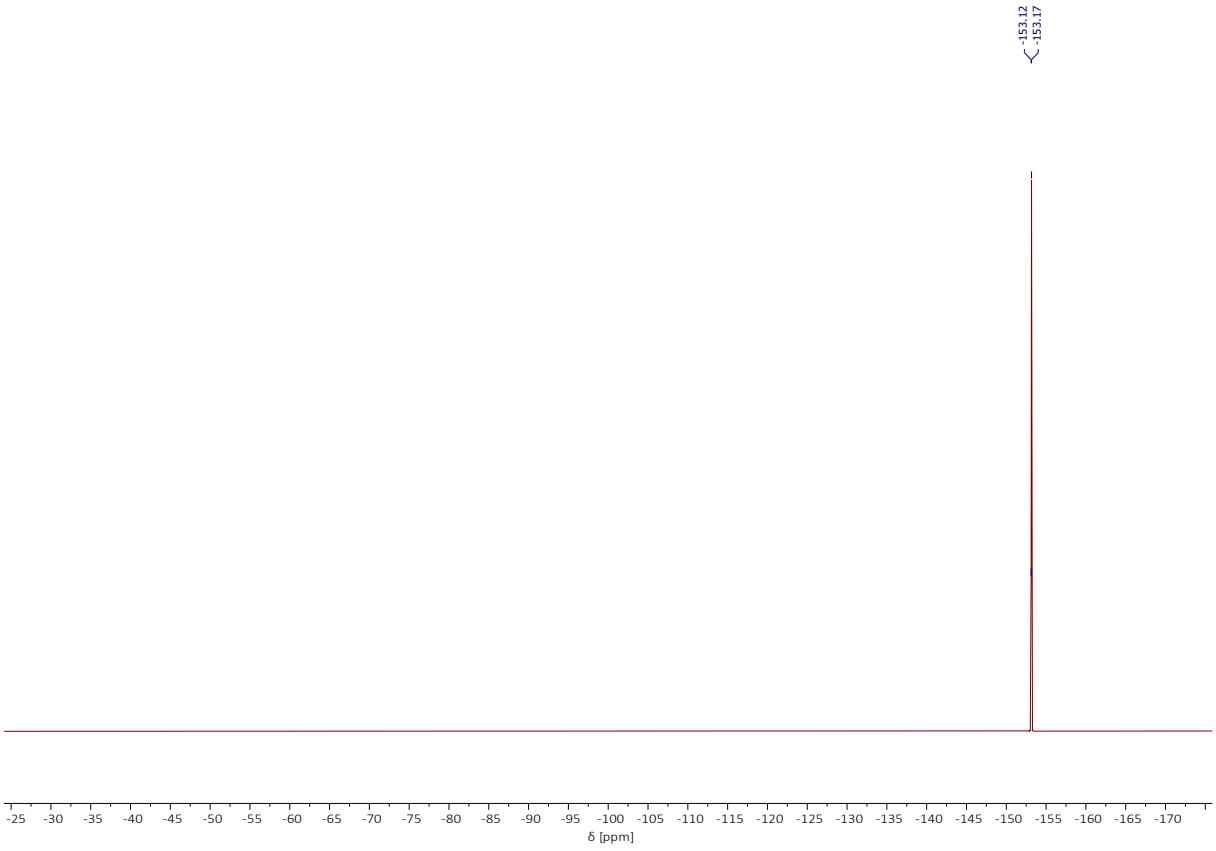

*Figure S46: $^{19}F\{^{1}H\}$-NMR spectrum (471 MHz, 298 K) of **[CuL^{CC}L^{NN}]$^{+}$** in CD_2Cl_2.*

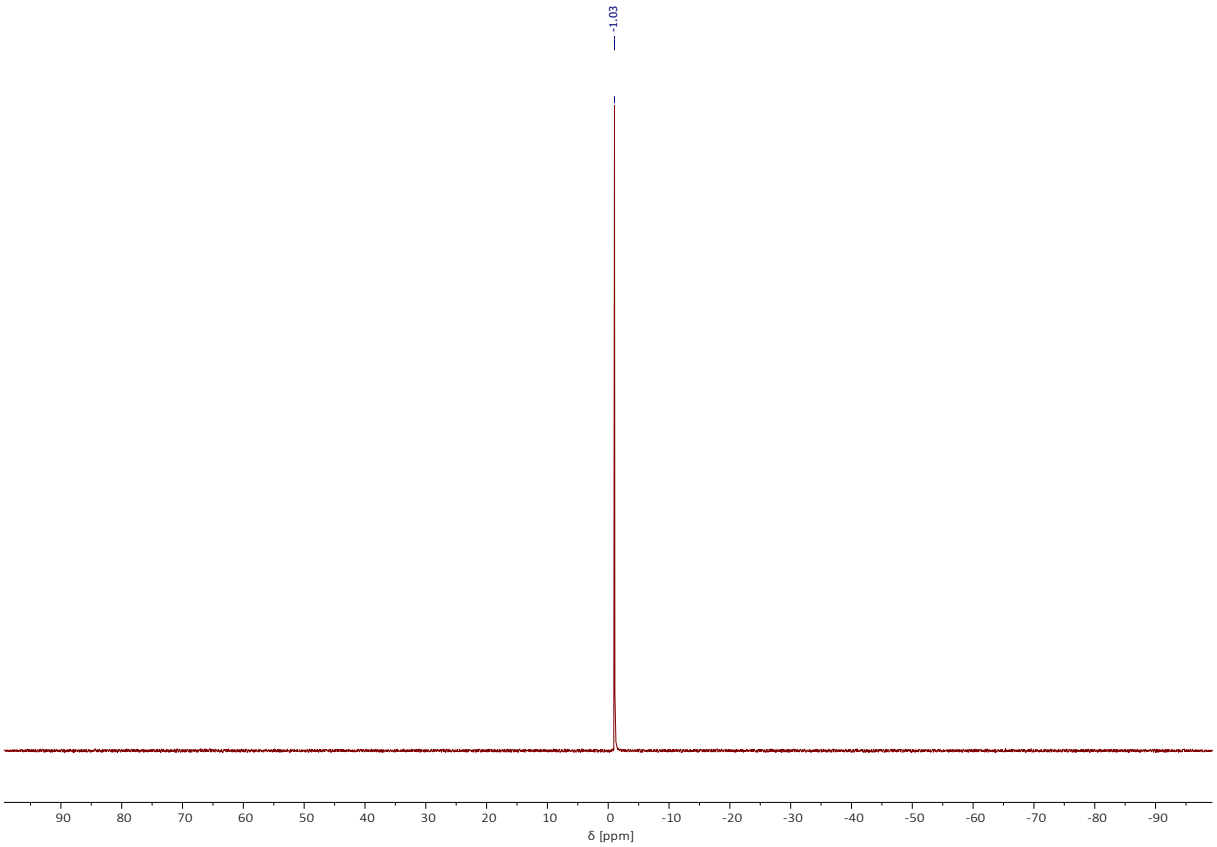

*Figure S 47: ^{11}B-NMR spectrum (128 MHz, 298 K) of **[CuL^{CC}L^{NN}]$^{+}$** in CD_2Cl_2.*

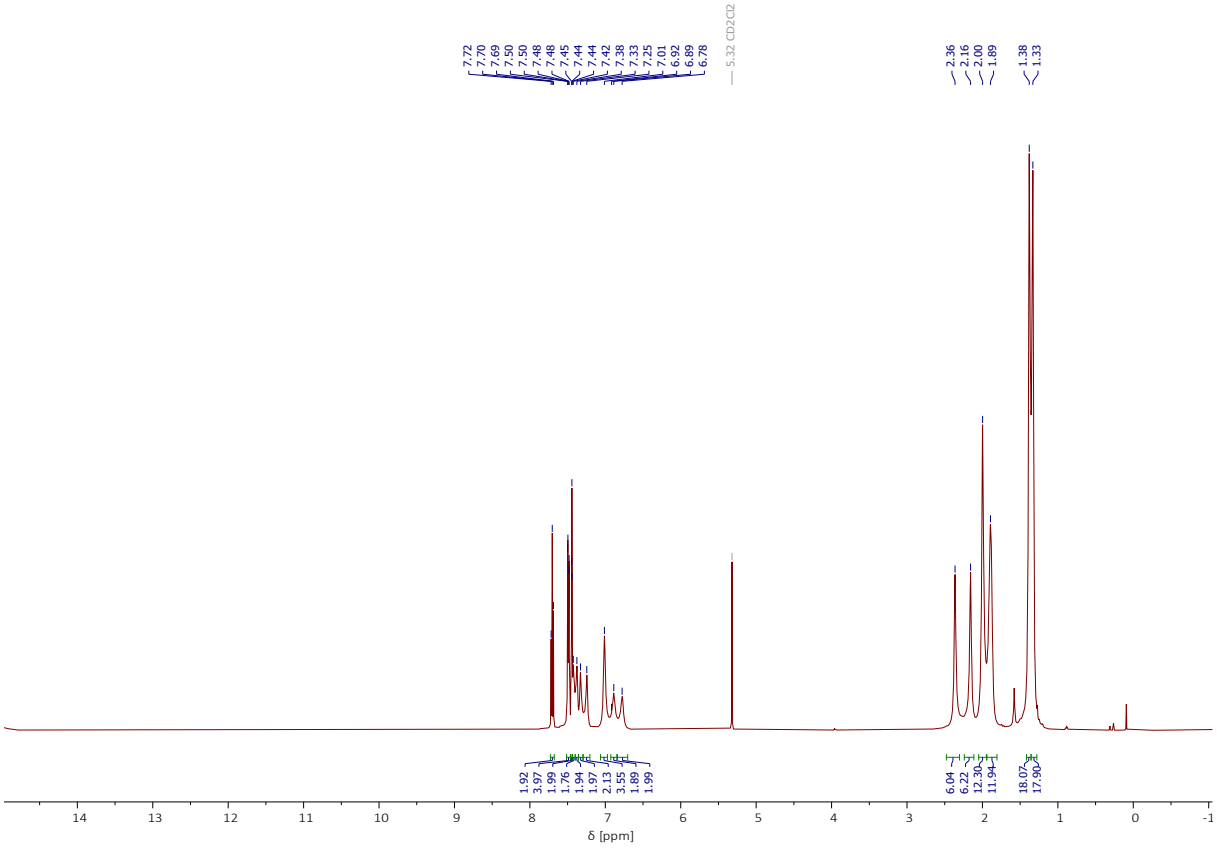

*Figure S48: ^{1}H-NMR spectrum (500 MHz, 298 K) of **[CuL^{CC}L^{CC}]$^{+}$** in CD_2Cl_2.*

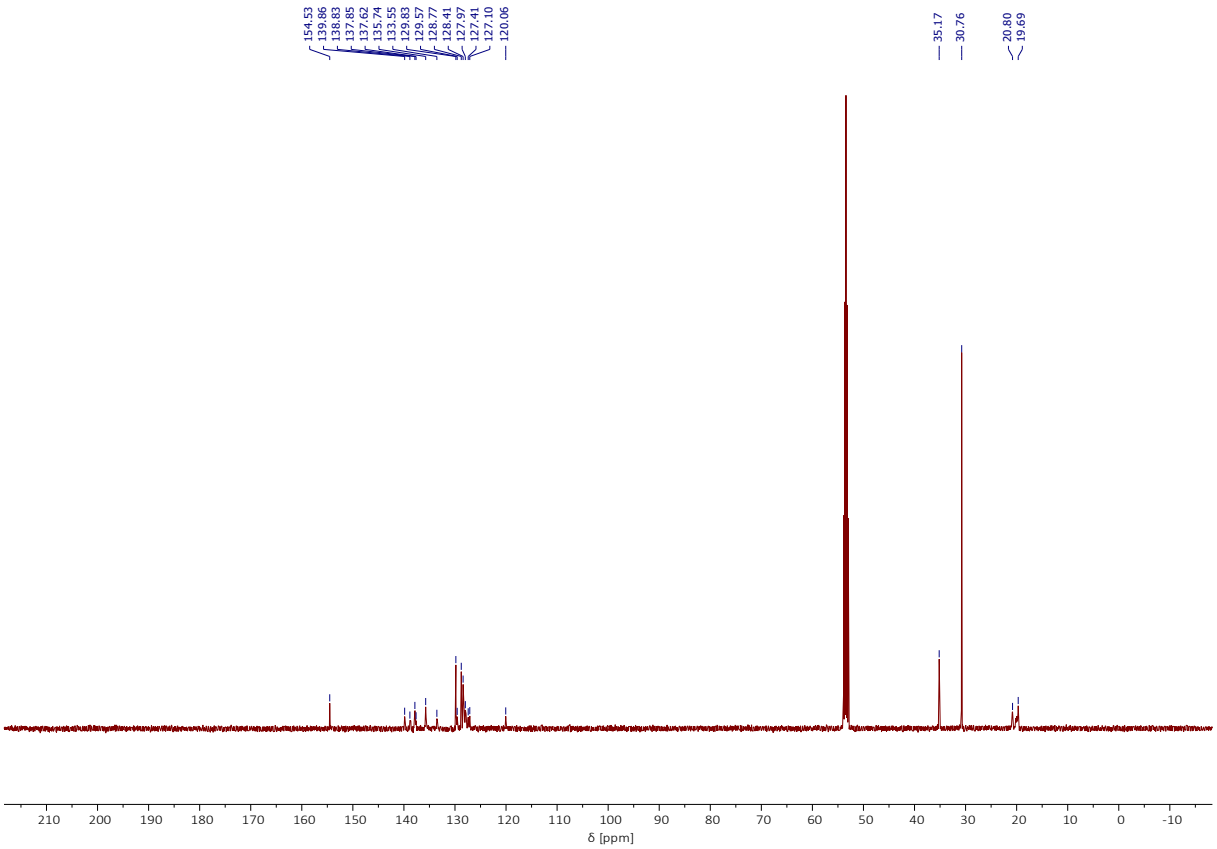

Figure S49: $^{13}C\{^1H\}$-NMR spectrum (126 MHz, 298 K) of ***[CuL^{CC}L^{CC}]$^+$*** *in CD_2Cl_2.*

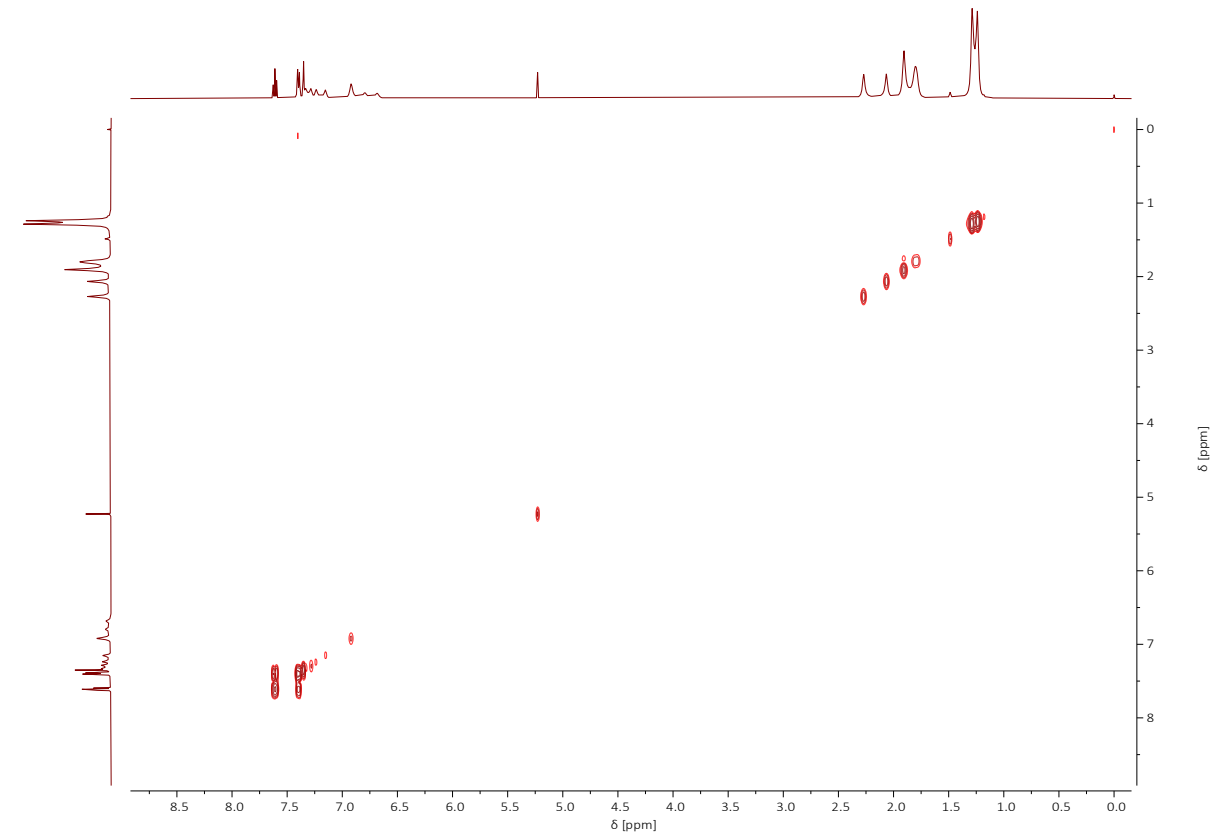

Figure S50: $^1H, ^1H$-COSY spectrum (500 MHz, 500 MHz, 298 K) of ***[CuL^{CC}L^{CC}]$^+$*** *in CD_2Cl_2.*

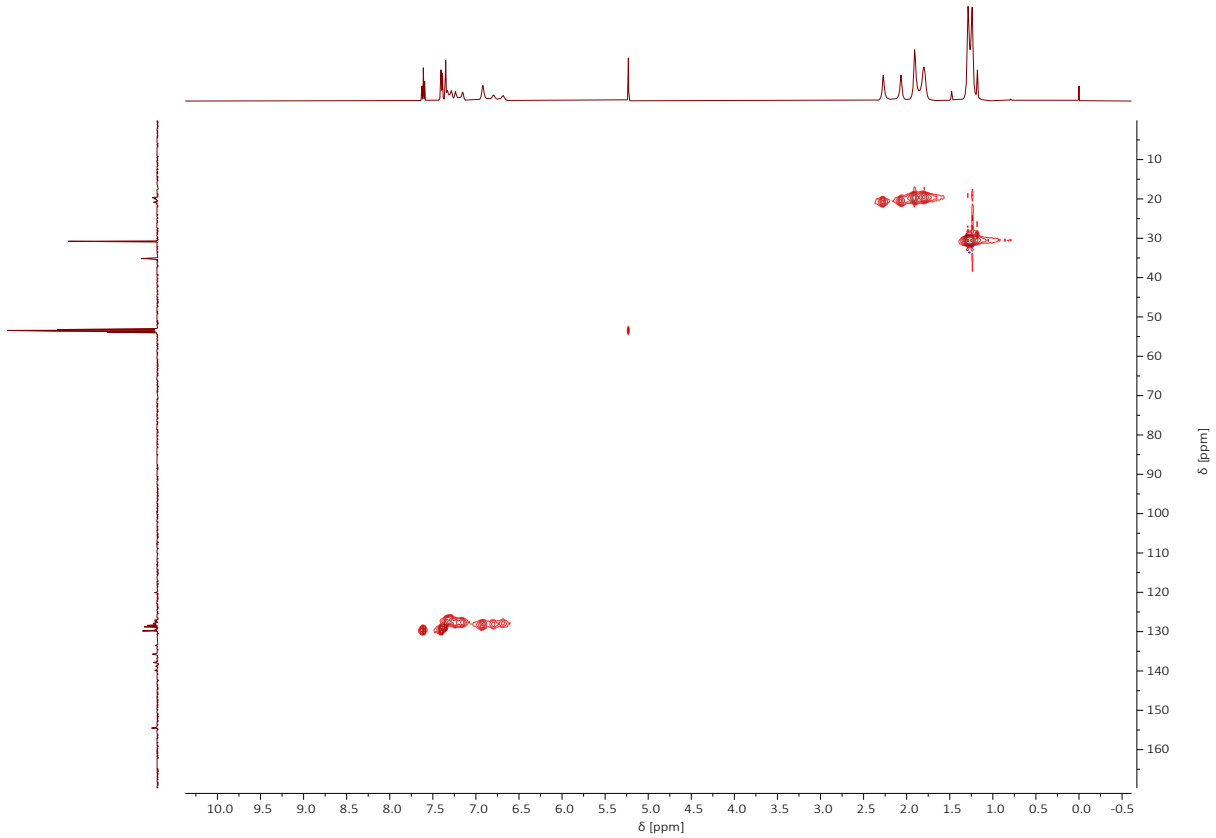

Figure S51: $^{1}H,^{13}C$-HMQC spectrum (500 MHz, 126 MHz, 298 K) of ***[CuL^{CC}L^{CC}]$^{+}$*** *in CD_2Cl_2.*

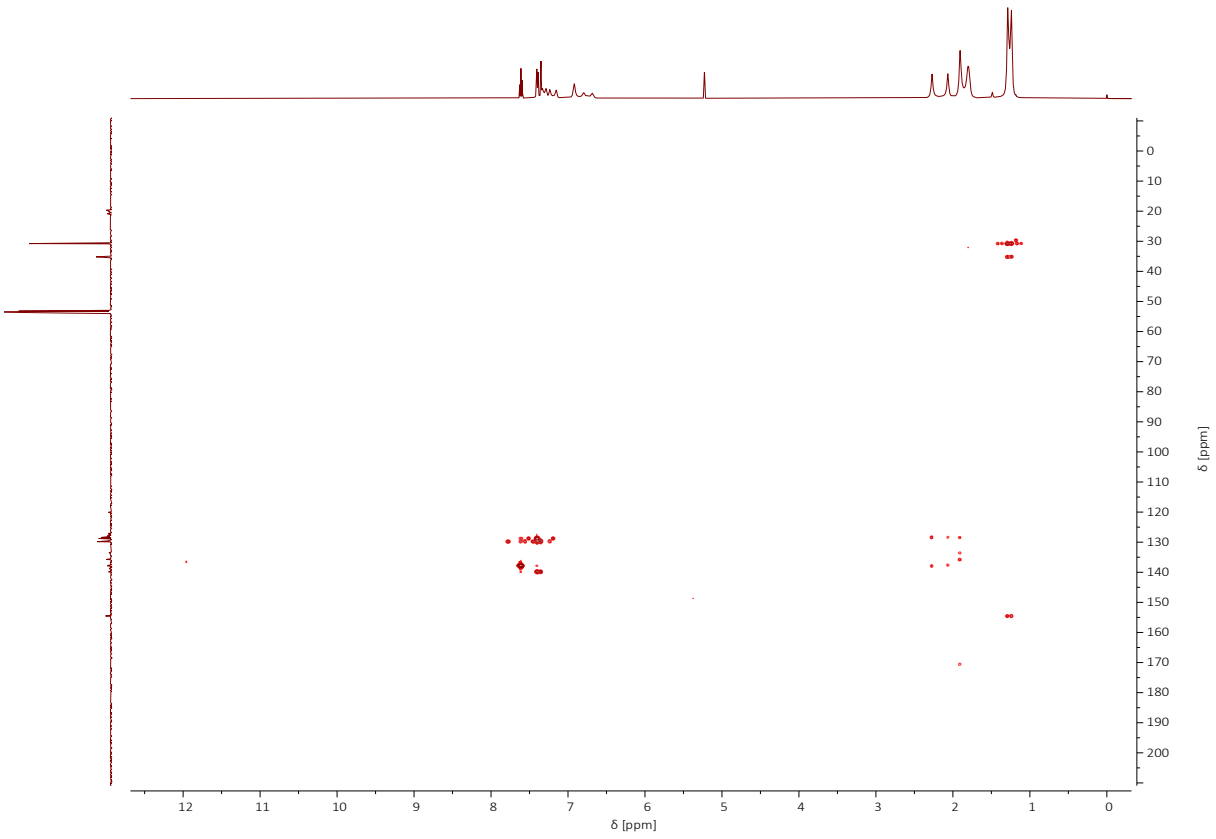

Figure S52: $^{1}H,^{13}C$-HMBC spectrum (500 MHz, 126 MHz, 298 K) of ***[CuL^{CC}L^{CC}]$^{+}$*** *in CD_2Cl_2.*

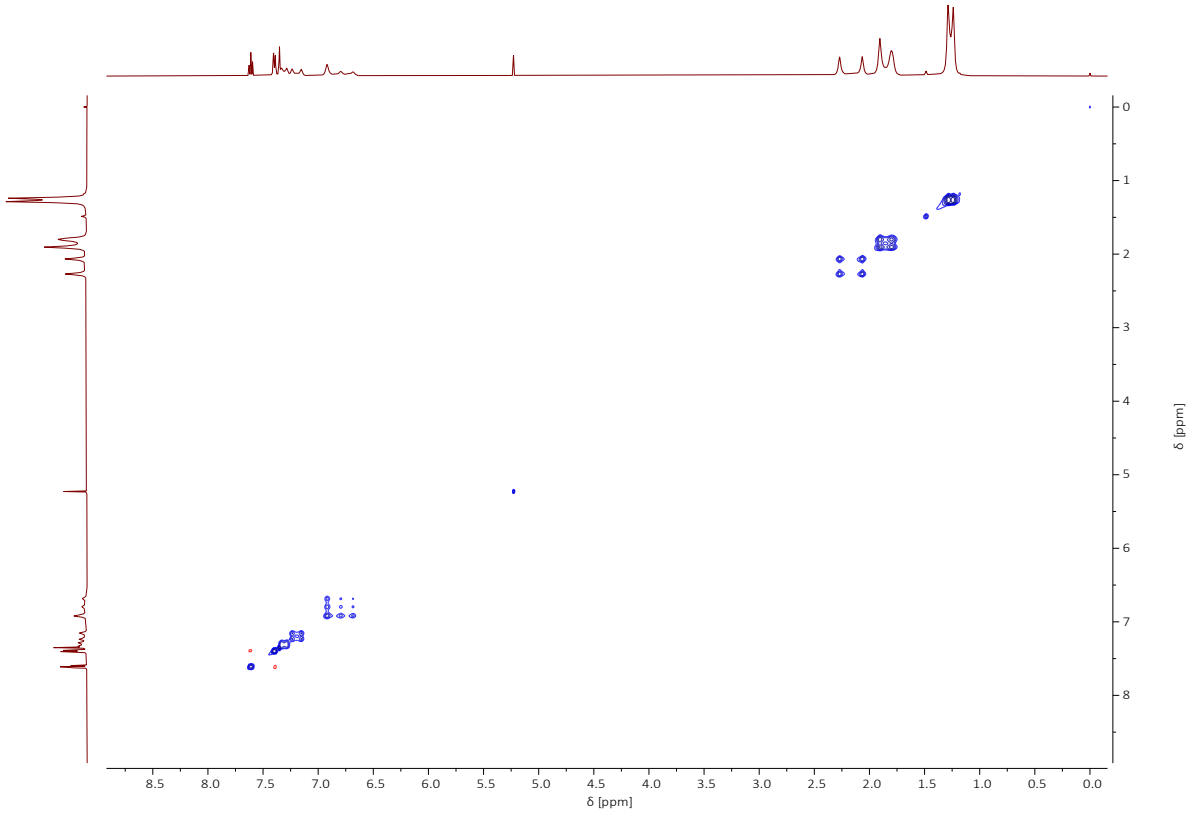

*Figure S53: $^{1}H,^{13}C$-NOESY spectrum (500 MHz, 126 MHz, 298 K) of **[CuL^{CC}L^{CC}]$^{+}$** in CD_2Cl_2.*

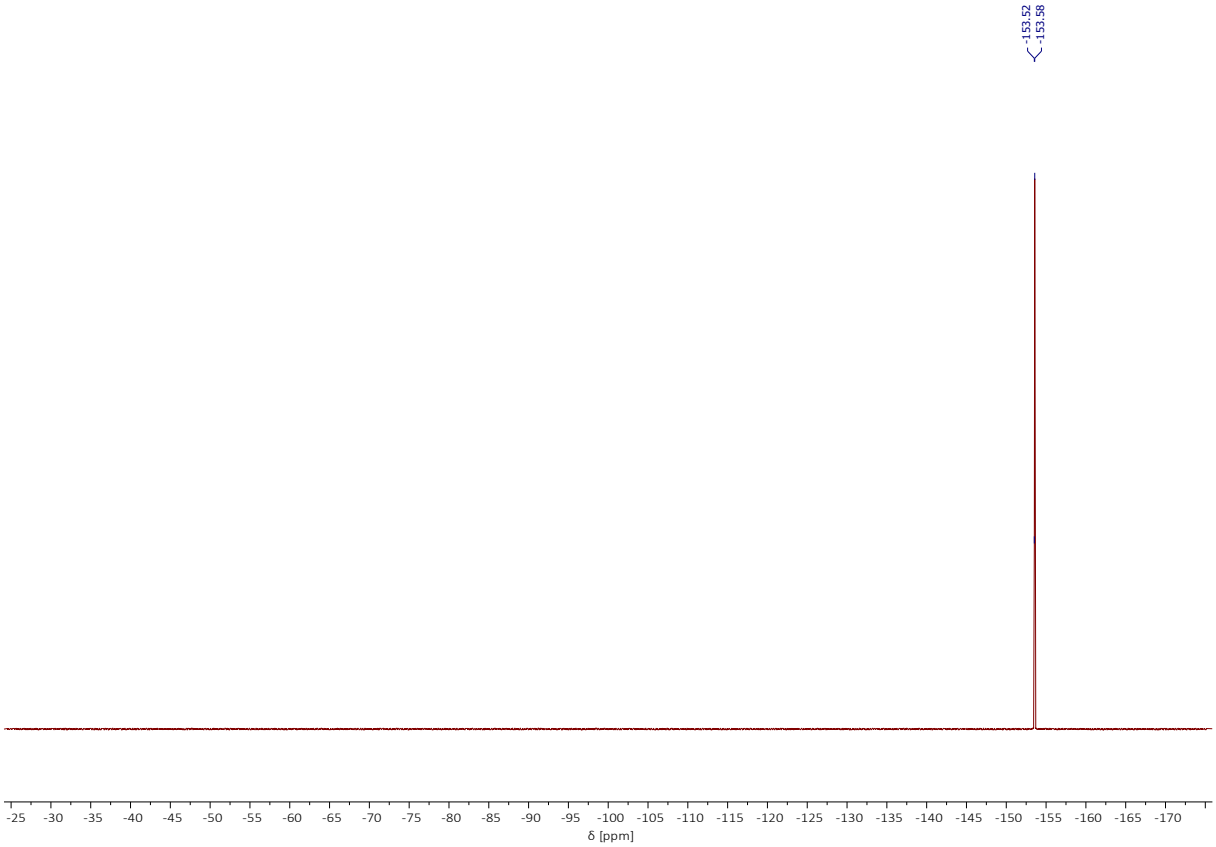

*Figure S54: $^{19}F\{^{1}H\}$-NMR spectrum (471 MHz, 298 K) of **[CuL^{CC}L^{CC}]$^{+}$** in CD_2Cl_2.*

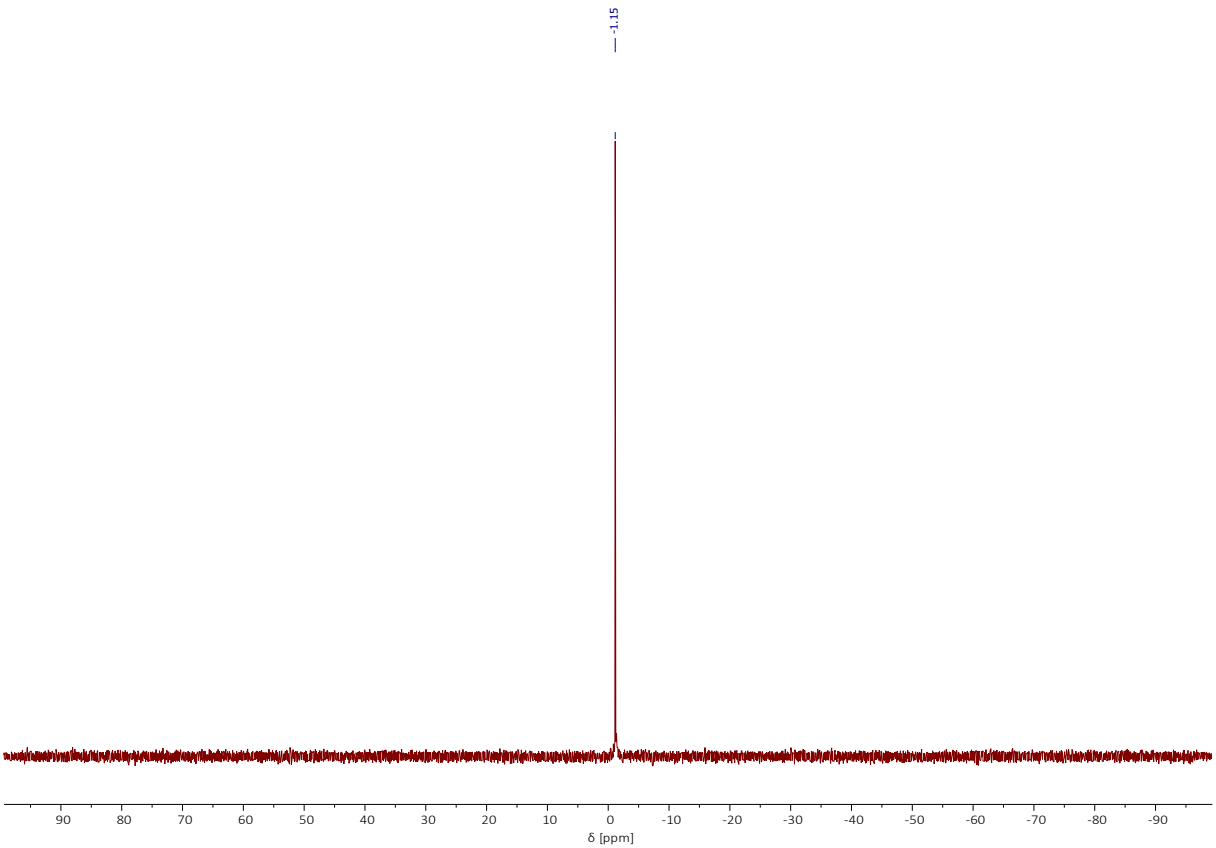

Figure S55: ^{11}B-NMR spectrum (128 MHz, 298 K) of ***[CuL^{CC}L^{CC}]$^{+}$*** *in CD_2Cl_2.*

10 High resolution mass spectra

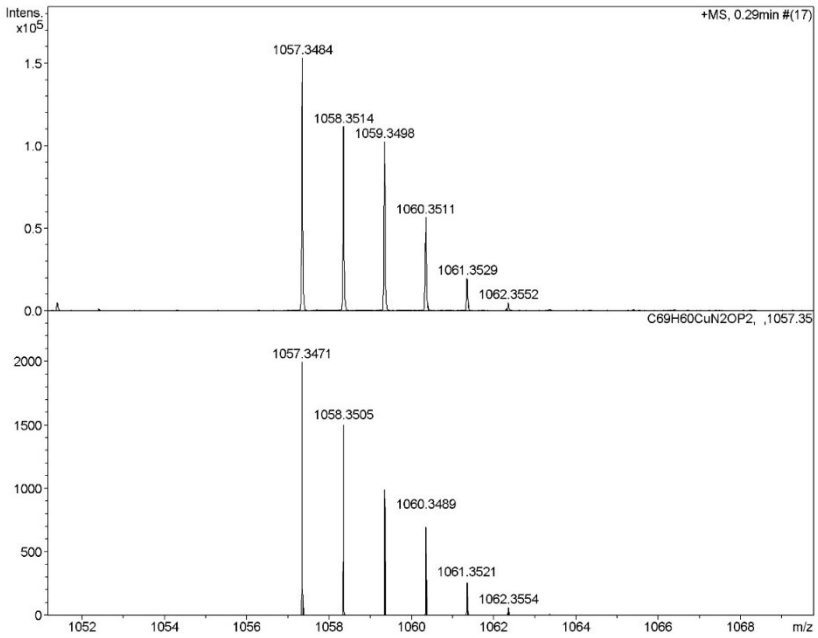

Figure S56: Top: ESI-HRMS (positive ions) of ***[CuL^{NN}L^{PP}]$^{+}$****. Bottom: Simulated spectrum for* ***[CuL^{NN}L^{PP}]$^{+}$****.*

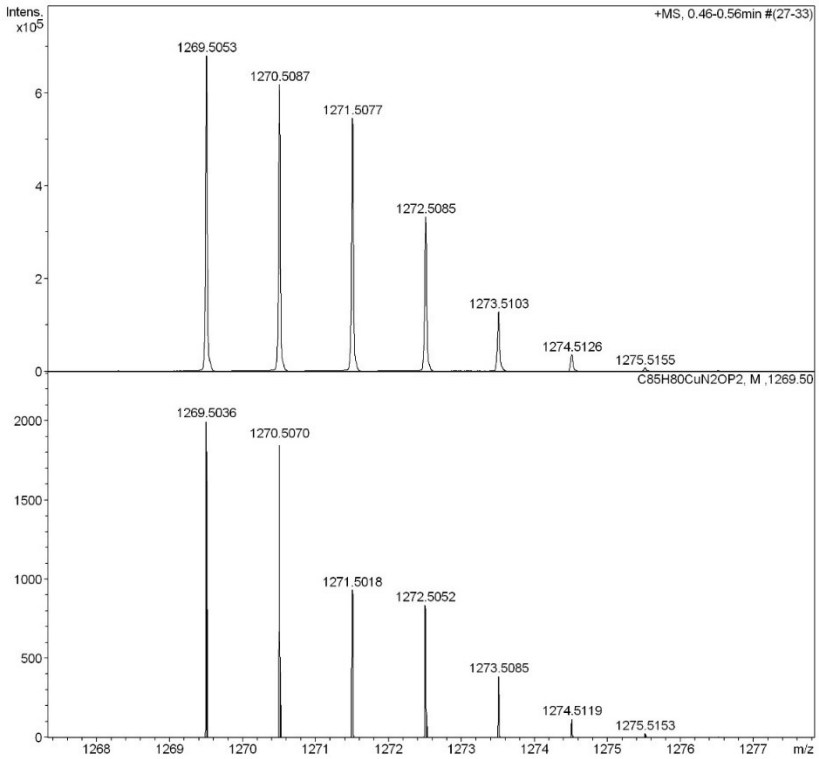

Figure S57: Top: ESI-HRMS (positive ions) of ***[CuL^{CC}L^{PP}]$^{+}$****. Bottom: Simulated spectrum for* ***[CuL^{CC}L^{PP}]$^{+}$****.*

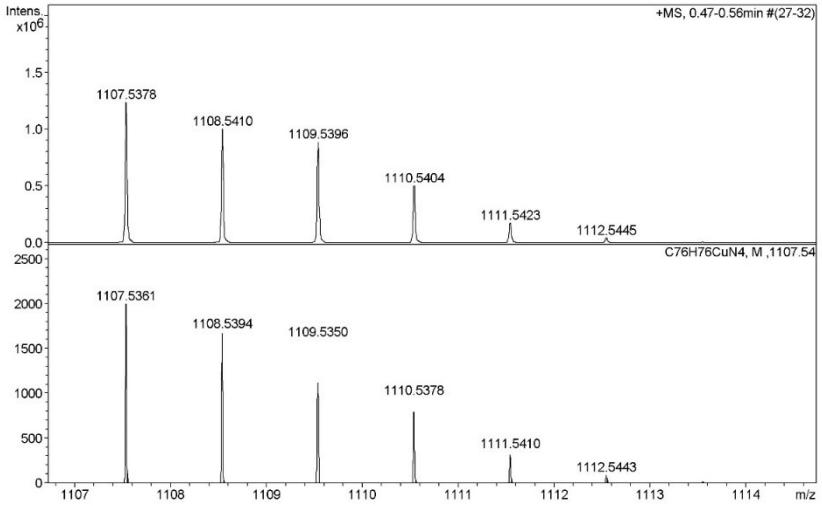

Figure S58: Top: ESI-HRMS (positive ions) of ***[CuL^{CC}L^{NN}]$^{+}$****. Bottom: Simulated spectrum for* ***[CuL^{CC}L^{NN}]$^{+}$****.*

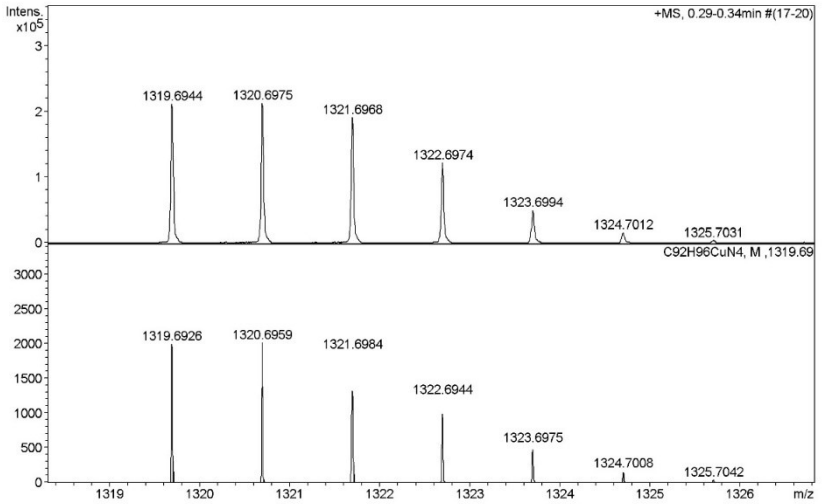

Figure S59: Top: ESI-HRMS (positive ions) of ***[CuL^{CC}L^{CC}]$^{+}$****. Bottom: Simulated spectrum for* ***[CuL^{CC}L^{CC}]$^{+}$****.*

11 References

1. L. Kohler, D. Hayes, J. Hong, T. J. Carter, M. L. Shelby, K. A. Fransted, L. X. Chen and K. L. Mulfort, *Dalton Trans.*, 2016, **45**, 9871–9883.
2. T. Rawner, E. Lutsker, C. A. Kaiser and O. Reiser, *ACS Catal.*, 2018, **8**, 3950–3956.
3. N. Sinha, C. Wegeberg, D. Häussinger, A. Prescimone and O. S. Wenger, *Nat. Chem.*, 2023, **15**, 1730–1736.
4. G. R. Fulmer, A. J. M. Miller, N. H. Sherden, H. E. Gottlieb, A. Nudelman, B. M. Stoltz, J. E. Bercaw and K. I. Goldberg, *Organometallics*, 2010, **29**, 2176–2179.
5. G. M. Sheldrick, *Acta Crystallogr. A*, 2015, **71**, 3–8.
6. O. V. Dolomanov, L. J. Bourhis, R. J. Gildea, J. A. K. Howard and H. Puschmann, *J. Appl. Crystallogr.*, 2009, **42**, 339–341.
7. G. M. Sheldrick, *Acta Crystallogr. C.*, 2015, **71**, 3–8.
8. L. Yang, D. R. Powell and R. P. Houser, *Dalton Trans.*, 2007, 955–964.
9. F. Xu, T. Tao, K. Zhang, X. X. Wang, W. Huang and X. Z. You, *Dalton Trans.*, 2013, **42**, 3631–3645.
10. Y. Yang, F. Doettinger, C. Kleeberg, W. Frey, M. Karnahl and S. Tschierlei, *Front Chem.*, 2022, **10**, 936863.
11. M. Knorn, T. Rawner, R. Czerwieniec and O. Reiser, *ACS Catal.*, 2015, **5**, 5186–5193.